Lattice Monte Carlo meets the lattice functional renormalization group: A quantitative comparison

Niklas Zorbach,[1,*] Jan Philipp Klinger,[2,†] Owe Philipsen,[2,‡] and Jens Braun[1,3,4,§]

[1]*Department of Physics, Institut für Kernphysik, Theoriezentrum, Technische Universität Darmstadt, Schlossgartenstraße 2, D-64289 Darmstadt, Germany*

[2]*Institute for Theoretical Physics, Goethe-University Frankfurt am Main, Max-von-Laue-Strasse 1, 60438 Frankfurt am Main, Germany*

[3]*Helmholtz Research Academy Hesse for FAIR, Campus Darmstadt, D-64289 Darmstadt, Germany*

[4]*ExtreMe Matter Institute EMMI, GSI, Planckstraße 1, D-64291 Darmstadt, Germany*

(Received 26 May 2025; accepted 3 September 2025; published 31 October 2025)

Lattice Monte Carlo simulations and the functional renormalization group (RG) are powerful approaches that allow for quantitative studies of nonperturbative phenomena such as bound-state formation, spontaneous symmetry breaking, and phase transitions. While results from both methods have recently shown remarkable agreement for many observables, e.g., in quantum chromodynamics, an analysis of deviations in certain quantities turns out to be challenging. This is because calculations with the two methods are based on different approximations, regularizations, and scale fixing procedures. In the present work, we present a framework for a more direct comparison by formulating the functional RG approach on a finite spacetime lattice. This removes all ambiguities of regularization, finite-size, and scale fixing procedures in concrete studies. By investigating the emergence of spontaneous symmetry breaking and phase transitions in a $Z(2)$ scalar theory in $d = 1$, 2, and 3 spacetime dimensions, we demonstrate at the example of the local potential approximation how this framework can be used to evaluate and compare the systematic errors of both approaches.

DOI: 10.1103/nsd5-nxdp

I. INTRODUCTION

Phase transitions in strongly coupled systems are intensively studied in many areas of research and require nonperturbative methods to arrive at reliable theoretical predictions. One example is quantum chromodynamics (QCD), whose phase structure is relevant for the early Universe, heavy-ion collisions, and neutron star physics. In recent years, investigations at high temperature and low densities have been pushed to a new level with first-principles calculations, see, e.g., Refs. [1–17] for recent lattice QCD studies, Refs. [18–25] for recent first-principles studies based on functional approaches, and Refs. [26–29] for reviews. While both approaches are inherently nonperturbative, they have complementary systematic errors, strengths, and weaknesses. This motivates a systematic understanding of the former by detailed comparisons.

Although results from lattice QCD calculations and first-principles functional studies show remarkable agreement for many observables, an analysis of the origin of differences remains difficult, due to the many possible sources, such as different implementations of the QCD action and its symmetries, cutoff effects, finite-volume effects, and truncations. Moreover, different scale fixing procedures are often used in lattice Monte Carlo (MC) and functional studies which potentially results in a nontrivial matching procedure for the parameters of the theory under consideration. However, for a quantitative comparison and a rigorous understanding of the effect of approximations, it is necessary to eliminate any nontrivial matching procedure for parameters.

In this work we aim to overcome some of these problems by formulating the functional renormalization group (RG) approach on a finite spacetime lattice. This allows us to trivially relate the bare actions entering lattice MC and functional renormalization group (fRG) studies and, in particular, obviates a continuum limit before a meaningful comparison. As a first step, we restrict ourselves to a scalar theory without gauge degrees of freedom. This provides a useful framework for a quantitative analysis of the effect of

*Contact author: niklas.zorbach@tu-darmstadt.de
†Contact author: klinger@itp.uni-frankfurt.de
‡Contact author: philipsen@itp.uni-frankfurt.de
§Contact author: jens.braun@tu-darmstadt.de

a plethora of artifacts which are also present in QCD studies, such as cutoff artifacts, finite-volume effects, and truncation artifacts. Artifacts associated with different fermion implementations in lattice simulations may in principle be analyzed within such a framework as well. Moreover, the possibility of a clear comparison between the two methods is appealing as it may trigger a cross-fertilization with respect to improvements of both methods.

Based on earlier fRG studies of quantum field theories in a finite spacetime volume [30–34] and on a spacetime lattice [35–39], we set up a framework for clean direct comparisons of lattice MC and fRG studies, which allows for a quantitative understanding of the effect of the approximations underlying these two methods. This is of particular relevance for QCD applications but also beyond. For concreteness, we shall focus on a $Z(2)$ scalar field theory in $d = 1, 2, 3$ spacetime dimensions in the present work since it is simulable with high precision and allows for particularly clean comparisons of this kind. The consideration of different numbers of spacetime dimensions is interesting as it allows us to directly test whether a nontrivial momentum dependence in correlation functions is indeed suppressed when the number of spacetime dimensions is increased. Because of dimensional reduction, the case of spin-type models in $d = 3$ is of particular interest for QCD at finite temperature. For example, $O(4)$-type models are expected to provide an effective description of the chiral QCD phase transition at low densities and the restoration of the $Z(2)$ symmetry may play a prominent role close to a potentially existing critical end point in the QCD phase diagram.

This work is organized as follows: In Sec. II, we introduce the concrete model for our numerical studies. The two methods considered in our present work, lattice MC and lattice fRG, are then discussed in Secs. III and IV, respectively. While we keep the general introduction of the lattice MC approach brief, we provide a more detailed discussion of the lattice fRG approach. In general, the latter provides us with a set of differential equations for correlation functions on a spacetime lattice. In addition to a discussion of regulator functions, general aspects of RG flows on a spacetime lattice, and the connection to the standard continuum fRG approach, we discuss the truncation underlying our numerical calculations and show in which limits this truncation already provides us with exact results. To be specific, we consider the so-called local potential approximation (LPA) in our numerical studies which corresponds to the leading-order approximation in terms of a derivative expansion of the effective action. Note that this truncation is the simplest truncation in the fRG approach which already includes fluctuation effects. Our main results are presented in Sec. V, where we also provide an intrinsic estimate of the uncertainties of LPA by a direct computation of momentum-dependent corrections to the two-point function. In addition, we compare lattice MC and fRG results for the order parameter of our $Z(2)$ model and the susceptibility across lattices with different sizes. Our conclusions can be found in Sec. VI.

II. MODEL

We consider a single-component real scalar field ϕ on a d-dimensional isotropic lattice $\mathcal{V} = \{\boldsymbol{x} = (x_1, \ldots, x_d) | x_\mu = a n_\mu, n_\mu \in \{0, \ldots, N_\mu - 1\}\} \subset (a\mathbb{Z})^d$ with lattice spacing a and periodic boundary conditions for ϕ. The extent of the lattice is assumed to be the same in all directions, $N_\mu = N_\sigma$. The partition function reads

$$\mathcal{Z}[J] = \int \mathcal{D}\phi e^{-S[\phi] + J\cdot\phi}, \tag{1}$$

where $J \cdot \phi = a^d \sum_{\boldsymbol{x}\in\mathcal{V}} J_{\boldsymbol{x}}\phi_{\boldsymbol{x}}$, $S[\phi] = S(\{\phi_{\boldsymbol{x}\in\mathcal{V}}\})$,[1] and the measure of the partition function is defined as

$$\int \mathcal{D}\phi = \prod_{\boldsymbol{y}\in\mathcal{V}} a^{d_\phi} \int_{-\infty}^{\infty} \mathrm{d}\phi_{\boldsymbol{y}}. \tag{2}$$

Here, $d_\phi = (d-2)/2$ is the mass dimension of the field ϕ. Note that, with this definition of the measure, the path integral is dimensionless.

Furthermore, we work with a discretized bare action $S[\phi]$ of the following form:

$$S[\phi] = a^d \sum_{\boldsymbol{x}\in\mathcal{V}} \left[\frac{1}{2}\sum_{\mu=1}^{d} \Delta_\mu^f \phi_{\boldsymbol{x}} \Delta_\mu^f \phi_{\boldsymbol{x}} + \mathcal{U}(\phi_{\boldsymbol{x}})\right], \tag{3}$$

where $\Delta_\mu^f \phi_{\boldsymbol{x}} = (\phi_{\boldsymbol{x}+\boldsymbol{e}_\mu} - \phi_{\boldsymbol{x}})/a$ is the discretized forward derivative and $\mathcal{U}(\phi_{\boldsymbol{x}})$ denotes the bare potential of the form

$$\mathcal{U}(\phi_{\boldsymbol{x}}) = \frac{1}{2} m^2 \phi_{\boldsymbol{x}}^2 + \frac{1}{4!}\lambda\phi_{\boldsymbol{x}}^4 - c\phi_{\boldsymbol{x}}. \tag{4}$$

Here, we introduced an external homogeneous field c which couples linearly to the field ϕ. For the quartic coupling we assume $\lambda > 0$.

By rewriting the kinetic part of the action (3) in momentum space, we find

$$S[\phi] = \frac{1}{V}\sum_{\boldsymbol{q}\in\tilde{\mathcal{V}}} \frac{\epsilon_{\boldsymbol{q}}^2}{2} \tilde{\phi}_{-\boldsymbol{q}}\tilde{\phi}_{\boldsymbol{q}} + a^d \sum_{\boldsymbol{x}\in\mathcal{V}} \mathcal{U}(\phi_{\boldsymbol{x}}), \tag{5}$$

where $V = (aN_\sigma)^d$ denotes the volume of the system and $\tilde{\mathcal{V}} = \{\boldsymbol{q} = (q_1, \ldots, q_d) | q_\mu = \frac{2\pi n_\mu}{aN_\sigma}, n_\mu \in \{0, \ldots N_\sigma - 1\}\}$ the corresponding momentum space. The kinetic energy $\epsilon_{\boldsymbol{q}}$ is defined as

[1]From here on, $A[\phi]$ is short for $A(\{\phi_{\boldsymbol{x}\in\mathcal{V}}\})$.

$$\epsilon_{\boldsymbol{q}}^2 = \sum_{\mu=1}^{d} \left[\frac{2}{a}\sin\left(\frac{1}{2}aq_\mu\right)\right]^2. \tag{6}$$

This quantity determines the kinetic energy levels for a given lattice momentum $\boldsymbol{q}$. Note that the functional form of the kinetic energy reflects the periodic boundary conditions.

A. Spontaneous symmetry breaking

Spontaneous symmetry breaking (SSB) of the global $Z(2)$ symmetry of our theory can be realized only in the thermodynamic limit, $N_\sigma \to \infty$ (for a fixed lattice spacing). In any finite volume quantum fluctuations inevitably restore the $Z(2)$ symmetry. From a mathematical standpoint, SSB can be defined as a limiting process where an external $Z(2)$ symmetry breaking source (e.g., given in form of the parameter c in our action above) is removed *after* the extrapolation to the infinite volume limit has been taken.

An order parameter for spontaneous $Z(2)$ symmetry breaking is given by the "magnetization,"

$$\langle M\rangle \coloneqq \lim_{c\to 0}\lim_{V\to\infty}\langle M\rangle_{V,c}, \tag{7}$$

where M is the average field value

$$M = \frac{a^d}{V}\sum_{\boldsymbol{x}\in\mathcal{V}}\phi_{\boldsymbol{x}}, \tag{8}$$

and $\langle\cdot\rangle_{V,c}$ is the expectation value with respect to the partition function (1) for a system in a volume V in the presence of an external field c. The $Z(2)$ symmetry is said to be spontaneously broken, if $\langle M\rangle \neq 0$ for a given fixed lattice spacing.

Whether the $Z(2)$ symmetry can be spontaneously broken in the ground state at all depends on the number of spacetime dimensions. To be specific, the Mermin-Wagner theorem forbids SSB in $d < 2$ spacetime dimensions which results in a vanishing magnetization, i.e., $\langle M\rangle = 0$ for $d < 2$, regardless of the exact values of the model parameters. Note that, for theories with a continuous symmetry, such as $O(N > 1)$, there is no SSB even in $d = 2$ spacetime dimensions due to the presence of massless Nambu-Goldstone bosons.

We emphasize that the role of the explicit symmetry breaking term in the definition of the magnetization (7) is crucial, since it distinguishes a direction in field space along which the formation of a nontrivial minimum is energetically favored, such that $\langle M\rangle_{V,c>0} > 0$. Without external field c, the magnetization would vanish for all finite volumes, i.e., $\langle M\rangle_{V,c=0} = 0$, and consequently, the limit in Eq. (7) would vanish for all bare actions with a global $Z(2)$ symmetry, regardless of the number of spacetime dimensions.

Quantum fluctuations associated with bosonic degrees of freedom tend to restore the symmetry in the ground state. Therefore, it is necessary (but not sufficient) to choose $m^2 < 0$ in Eq. (3) in order to obtain a ground state in the full quantum theory which is governed by spontaneous $Z(2)$ symmetry breaking. Indeed, provided m^2 has been chosen smaller than a critical value which depends on the parameters d and λ, the magnetization remains finite in $d \geq 2$ spacetime dimensions, even after all quantum fluctuations have been integrated out.

B. Effective potential

Many physical observables of our model can be directly extracted from the effective potential U, which is the potential contribution of the effective action for vanishing external fields, $c = 0$. The effective potential inherits the $Z(2)$ symmetry of the bare action and is given by the Legendre transform of the Schwinger functional $W = \ln\mathcal{Z}$ at $c = 0$ evaluated at a constant field configuration $\boldsymbol{\phi} = (\phi_{\boldsymbol{x}})_{\boldsymbol{x}\in\mathcal{V}} = (\varphi,\ldots,\varphi)$,[2]

$$U(\varphi) = \frac{1}{V}\sup_{J}\Big(\boldsymbol{\phi}\cdot J - W_{c=0}[J]\Big). \tag{9}$$

Assuming the field configuration at the supremum J_{sup} is homogeneous, $J_{\text{sup}} = (j,\ldots,j)$,[3] the supremum over J can be replaced by a one-dimensional supremum over j. In this case, together with $\boldsymbol{\phi}\cdot J = V\varphi j$, Eq. (9) can be rewritten as

$$U(\varphi) = \frac{1}{V}\sup_{j}\Big(V\varphi j - W_{c=0}[J = (j,\ldots,j)]\Big). \tag{10}$$

Now we can utilize that the parameter c in the potential (4) enters the partition function in the same way as the source term, i.e., $W_{c=0}[J = (j,\ldots,j)] \equiv W_{c=j}[J = 0]$, to remove the source, implying that the effective potential (9) can be equivalently obtained from

$$U(\varphi) = \frac{1}{V}\sup_{c}\Big(V\varphi c - W_c[0]\Big). \tag{11}$$

[2]The quantity $\boldsymbol{\phi}$ should not be confused with a field vector as encountered in $O(N)$ models. The entries φ of this tuple are associated with the spacetime points $\boldsymbol{x}$ and assume the same value at all spacetime points in case of a constant field configuration.

[3]This assumption is in general only true when the condensate is homogeneous for all c, i.e., when $\langle\phi_{\boldsymbol{x}}\rangle_{V,c} = \varphi$ for all $\boldsymbol{x}\in\mathcal{V}$. Then, we find

$$\varphi = \langle\phi_{\boldsymbol{x}}\rangle_{V,c} = a^{-d}\left.\frac{\partial W}{\partial J_{\boldsymbol{x}}}\right|_{J=(c,\ldots,c)}.$$

In particular, this holds if the ground state of the quantum theory is translation invariant.

Furthermore, since the magnetization can be expressed as a derivative of the Schwinger functional with respect to the external field,

$$\langle M\rangle_{V,c} = \frac{1}{V}\frac{\partial}{\partial c} W, \tag{12}$$

we conclude, together with Eq. (11), that

$$\partial_\varphi U(\langle M\rangle_{V,c}) = c. \tag{13}$$

From Eq. (13), we can already infer some general properties of the $Z(2)$-symmetric effective potential in both finite and infinite volume. In finite volume the effective potential is strictly convex with a trivial global minimum at $\varphi = 0$, since $\langle M\rangle_{V,c} \to 0$ as $c \to 0$. Only in the thermodynamic limit, $V \to \infty$, when a nontrivial magnetization persists as $c \to 0$, the effective potential U has two degenerate nontrivial minima located at $\pm\varphi_0$ which must also coincide with the magnetization (7), i.e., $\varphi_0 \equiv \langle M\rangle$.

Moreover, Eq. (13) can be used to reconstruct the effective potential and its derivative, $\partial_\varphi U(\varphi)$, by performing multiple calculations of the magnetization for different values of c, see also Refs. [21,23]. This approach is exactly what we employ in our analysis of finite systems in Sec. V B.

Another physically relevant quantity which we will discuss in Sec. V B is the so-called susceptibility, which is the integrated connected two-point correlation function and can be expressed by the magnetization,

$$\chi_{V,c} = V\langle (M - \langle M\rangle_{V,c})^2\rangle_{V,c}. \tag{14}$$

This quantity diverges at second-order phase transitions in the thermodynamic limit and hence can be used to identify these. In terms of the Schwinger functional, it can be written as the second derivative with respect to the external field c,

$$\chi_{V,c} = \frac{1}{V}\frac{\partial^2}{\partial c^2} W, \tag{15}$$

which, using Eqs. (12) and (13), implies

$$\partial^2_\varphi U(\langle M\rangle_{V,c}) = \chi^{-1}_{V,c}. \tag{16}$$

Thus, the susceptibility is associated with the inverse curvature of the effective potential evaluated at the corresponding magnetization $\varphi = \langle M\rangle_{V,c}$. In finite volumes, the susceptibility can never diverge as the effective potential is strictly convex, regardless of the number of spacetime dimensions or the specific values of m^2 and $\lambda > 0$ in the bare potential.

III. LATTICE MC SIMULATIONS

The aim of this work is a direct comparison of lattice MC and lattice fRG calculations. By using the same discretized action on the same spacetime lattice with given lattice spacing and volume, we avoid any "translation" or renormalization of model parameters between the two approaches and, in particular, the necessity of a continuum limit.

For given lattice spacing, volume, and bare parameter sets, the only approximation of a MC simulation consists of evaluating the path integral on a finite (rather than infinite) number of field configurations. In a process referred to as importance sampling, a set of field configurations is generated with probability weights given by the Boltzmann factor $e^{-S[\phi]}$. The expectation value of a given observable $\mathcal{O}$ is then approximated as an average over the generated field configurations,

$$\langle \mathcal{O}\rangle_{V,c} \approx \frac{1}{N}\sum_{i=1}^{N} \mathcal{O}[\phi^i]. \tag{17}$$

Here, ϕ^i refers to a specific field configuration generated in the MC process. The fluctuation of the observable with the different configurations is evaluated by the usual standard deviation, which diminishes as $N^{-1/2}$ as the number of configurations is increased.

We generate our field configurations using a hybrid Monte Carlo (HMC) algorithm [40]. Furthermore, after every HMC step we include a sign flip $\phi \to -\phi$ with a subsequent accept-reject step. This ensures that the simulation does not get "stuck" in a specific minimum of the potential, thus reducing the initial correlation between consecutive configurations and therefore the overall simulation time. In order to control and further suppress correlations, we bin our data and calculate the statistical errors using the jackknife procedure. Since a scalar theory on the lattice is computationally not very demanding, the statistical uncertainty in the following results could be kept small by accumulating a large amount of uncorrelated data. Whenever not visible, error bars are smaller than the symbol sizes.

IV. LATTICE FUNCTIONAL RENORMALIZATION GROUP

Although the fRG method has originally been developed for studies of systems in infinitely large, continuous spacetime volumes, it is also suitable to study theories on finite spacetime lattices. This has been done in previous works on scalar field theories such as in Refs. [35–39]. Studies of systems of scalar field theories and fermion-boson models in a continuous but finite spacetime volume have been put forward in Refs. [30–33] which have been supplemented with an analysis of finite-temperature and density effects [41–43], see Ref. [44] for a review.

The underlying idea of the fRG approach is to integrate out the momentum modes of the partition function successively, starting with the bare action (3). To this end, it is necessary to introduce an infrared regulator R_k which introduces a RG scale k into the theory. This regulator

suppresses modes with momenta $\epsilon_{\boldsymbol{q}} \lesssim k$ while modes with momenta $\epsilon_{\boldsymbol{q}} \gtrsim k$ are no longer affected by the regulator. In the path integral, the regulator appears in form of a regulator term,

$$\Delta S_k(\{\phi_{\boldsymbol{x}\in\mathcal{V}}\}) = \frac{1}{V}\sum_{\boldsymbol{q}\in\tilde{\mathcal{V}}} \frac{R_k(\epsilon_{\boldsymbol{q}})}{2}\tilde{\phi}_{-\boldsymbol{q}}\tilde{\phi}_{\boldsymbol{q}}, \tag{18}$$

which is added to the bare action S, see Refs. [45,46] for a general discussion of the properties of regulators. This yields the scale-dependent partition function $\mathcal{Z}_k$,

$$\mathcal{Z}_k[J] = \int \mathcal{D}\phi e^{-S[\phi]-\Delta S_k[\phi]+J\cdot\phi}, \tag{19}$$

from which the Wetterich equation can be derived in a similar way as for continuous spacetimes. The exact flow equation for the effective action in position space reads [45]

$$\partial_t\bar{\Gamma}_k[\phi] = a^{2d}\sum_{\boldsymbol{x},\boldsymbol{y}\in\mathcal{V}}\left(\bar{\Gamma}^{(2)}_{k,\boldsymbol{ab}}[\phi] + \Delta S^{(2)}_{k,\boldsymbol{ab}}\right)^{-1}_{\boldsymbol{xy}}\partial_t\Delta S^{(2)}_{k,\boldsymbol{yx}}, \tag{20}$$

where we have introduced the so-called scale-dependent effective average action $\bar{\Gamma}_k$.[4] Moreover, with the scale derivative $\partial_t = -k\partial_k$, we have implicitly introduced the quantity t which can be related to the so-called RG time. For reviews and introductions to the continuum formulation of the Wetterich equation, see Refs. [27,46–51].

The lattice formulation of the Wetterich equation (20) is a partial differential equation with $1+|\mathcal{V}|$ variables. Its solution, the scale-dependent effective average action $\bar{\Gamma}_k$, interpolates between the bare action $S[\phi]$ as $k\to\infty$ and the full quantum effective action $\Gamma[\phi]$ as $k\to 0$. The latter property of the scale-dependent effective action is trivially fulfilled, as Eq. (19) reduces to Eq. (1) when $k\to 0$. A more detailed derivation of the ultraviolet (UV) limit is shown in Sec. IV A 2. In the following, we refer to the limits $k\to\infty$ and $k\to 0$ as UV limit and infrared (IR) limit, respectively.

Formally, the Wetterich equation represents an initial value problem where the initial condition is given by an action $\bar{\Gamma}_\Lambda[\phi]$ at the so-called cutoff scale Λ and the differential equation is given by the Wetterich equation (20). As long as Λ is finite, this action is not identical to the bare action S. However, in the UV limit, the "running couplings" of the fRG flow, i.e., the couplings $\lambda_i(k)$ of $\bar{\Gamma}_k$, must approach the (finite) values of the corresponding couplings λ_i in the bare action S,

$$\lim_{k\to\infty}\lambda_i(k) = \lambda_i. \tag{21}$$

Consequently for large RG scales $k \gg 1/a$, we should observe that the change of the couplings with respect to the RG scale approaches zero, i.e.,

$$\partial_t\lambda_i(k) \approx 0 \quad \text{for } k \gg 1/a. \tag{22}$$

To obtain the full quantum effective action Γ, it is therefore sufficient to initialize the flow equation (20) with the action $\bar{\Gamma}_\Lambda = S$ at some large but finite cutoff. This also ensures that this initial condition *canonically* fulfills the requirement of RG consistency [52], i.e., the cutoff independence of the full quantum effective action. This is in contrast to continuum theories, where a nontrivial scale-dependent initial condition S_Λ must be determined to ensure that the full quantum effective action Γ remains unchanged as Λ is varied.

A. RG flow on finite spacetime lattices

In this subsection, we discuss several aspects of RG flows on finite spacetime lattices.

Depending on the dispersion relation, one obtains a finite set of kinetic energy levels, $\mathcal{E} = \{\epsilon_{\boldsymbol{q}}|\boldsymbol{q}\in\tilde{\mathcal{V}}\} = \{0, \Delta\epsilon, \ldots, \epsilon_{\max}\}$. Here, $\Delta\epsilon$ is the lowest nonzero kinetic energy level, i.e., $\Delta\epsilon = \min_{\boldsymbol{q}\in\tilde{\mathcal{V}}\setminus\boldsymbol{0}}(\epsilon_{\boldsymbol{q}})$. For example, for the relation (6), the highest kinetic energy level is $\epsilon_{\max} = 2\sqrt{d}/a$ and the lowest nonzero level is given by $\Delta\epsilon = 2\sin(\pi/N_\sigma)/a$. This allows us to divide the RG flow into three regimes: the UV regime with $k > \epsilon_{\max}$, the intermediate regime with $\Delta\epsilon \le k \le \epsilon_{\max}$, and the IR regime with $k < \Delta\epsilon$. It is important to note that the precise values of the boundaries of these regimes may shift when the regulator is changed. This is because the regulator itself defines the notion of the RG scale. However, for the Litim regulator [53,54],

$$R_k(\epsilon_{\boldsymbol{q}}) = (k^2 - \epsilon_{\boldsymbol{q}}^2)\Theta(k^2 - \epsilon_{\boldsymbol{q}}^2), \tag{23}$$

which we shall primarily use in this work, the boundaries of the different regimes are as defined above.

Before discussing the different regimes of the RG flow, we introduce useful definitions and relations which will help in analyzing the dynamics in these regimes below. We start by considering the Wetterich equation (20) in momentum space and exploit the fact that the regulator is diagonal in momentum space, cf. Eq. (18),

$$\partial_t\bar{\Gamma}_k[\phi] = \frac{1}{2}\frac{1}{V}\sum_{\boldsymbol{q}\in\tilde{\mathcal{V}}} G^{(2)}_{k,\boldsymbol{q},-\boldsymbol{q}}[\phi]\partial_t R_k(\epsilon_{\boldsymbol{q}}), \tag{24}$$

[4] We define the functional derivatives of the nth order acting on an action A on a spacetime lattice in position space as

$$A^{(n),\boldsymbol{x}_1\ldots\boldsymbol{x}_n}[J] = a^{-d}\frac{\partial}{\partial J_{\boldsymbol{x}_1}}\ldots a^{-d}\frac{\partial}{\partial J_{\boldsymbol{x}_n}}A[J],$$

and correspondingly in momentum space as

$$A^{(n),\boldsymbol{q}_1\ldots\boldsymbol{q}_n}[J] = V\frac{\partial}{\partial\tilde{J}_{\boldsymbol{q}_1}}\ldots V\frac{\partial}{\partial\tilde{J}_{\boldsymbol{q}_n}}A[J].$$

with the propagator

$$G^{(2)}_{k,\boldsymbol{p},\boldsymbol{q}}[\phi] = \left(\bar{\Gamma}^{(2)}_{k,\boldsymbol{ab}}[\phi] + \Delta S^{(2)}_{k,\boldsymbol{ab}}\right)^{-1}_{\boldsymbol{pq}}. \tag{25}$$

In general, the inversion of the regularized two-point function in momentum space is nontrivial, even on a finite spacetime lattice. However, employing that the system under consideration is translation invariant and evaluating the propagator (25) at a constant background field configuration, $\phi = (\phi_{\boldsymbol{x}})_{\boldsymbol{x}\in\mathcal{V}} = (\varphi, \ldots, \varphi)$, we have

$$G^{(2)}_{k,\boldsymbol{p},\boldsymbol{q}}[\phi] = G^{(2)}_{k}(\varphi, \boldsymbol{q}) V \delta_{\boldsymbol{p},-\boldsymbol{q}} \tag{26}$$

and therefore

$$G^{(2)}_{k}(\varphi, \boldsymbol{q}) = \frac{1}{\partial^2_\varphi U_k(\varphi) + \Delta\bar{\Gamma}^{(2)}_k(\varphi, \boldsymbol{q}) + R_k(\epsilon_{\boldsymbol{q}})}. \tag{27}$$

Here, we have divided $\bar{\Gamma}^{(2)}_{k,\boldsymbol{p},\boldsymbol{q}}[\phi] = \bar{\Gamma}^{(2)}_k(\varphi, \boldsymbol{q}) V \delta_{\boldsymbol{p},-\boldsymbol{q}}$ into a potential-like and a kineticlike contribution. For the potential-like contribution we have

$$\partial^2_\varphi U_k(\varphi) = \bar{\Gamma}^{(2)}_k(\varphi, \boldsymbol{0}), \tag{28}$$

where U_k corresponds to the potential term of the scale-dependent effective average action $\bar{\Gamma}_k$, i.e., $U_k(\varphi) = V^{-1}\bar{\Gamma}_k[\phi]$. All momentum-dependent terms are encoded in the kineticlike contribution,

$$\Delta\bar{\Gamma}^{(2)}_k(\varphi, \boldsymbol{q}) = \bar{\Gamma}^{(2)}_k(\varphi, \boldsymbol{q}) - \bar{\Gamma}^{(2)}_k(\varphi, \boldsymbol{0}). \tag{29}$$

1. Infrared regime

Using the Litim regulator (23) or any other regulator fulfilling the property

$$\partial_t R_k(\epsilon_{\boldsymbol{q}}) = 0 \quad \text{for } k \leq \epsilon_{\boldsymbol{q}}, \tag{30}$$

the Wetterich equation (24) yields

$$\partial_t \bar{\Gamma}_k[\phi] = \frac{1}{2}\frac{1}{V}\sum_{\substack{\boldsymbol{q}\in\tilde{\mathcal{V}} \\ \epsilon_{\boldsymbol{q}}<k}} G^{(2)}_{k,\boldsymbol{q},-\boldsymbol{q}}[\phi]\partial_t R_k(\epsilon_{\boldsymbol{q}}). \tag{31}$$

This choice of regulator canonically truncates the right-hand side of the Wetterich equation without assuming any approximation. This implies that in the IR regime, for $k < \Delta\epsilon$, only the zero mode contributes to the Wetterich equation, which reduces Eq. (31) to

$$\partial_t \bar{\Gamma}_k[\phi] = \frac{1}{2}\frac{1}{V} G^{(2)}_{k,\boldsymbol{0},\boldsymbol{0}}[\phi]\partial_t R_k(0). \tag{32}$$

Now, evaluating both sides of Eq. (32) at a constant background field configuration $\phi = (\varphi, \ldots, \varphi)$ and using the structure of the propagator (27) with $\Delta\bar{\Gamma}^{(2)}_k(\varphi, \boldsymbol{0}) = 0$, we find for the scale-dependent effective potential, $U_k(\varphi) = V^{-1}\bar{\Gamma}_k[\phi]$, the exact flow equation

$$\partial_t U_k(\varphi) = \frac{1}{V}\frac{\partial_t R_k(0)}{\partial^2_\varphi U_k(\varphi) + R_k(0)}. \tag{33}$$

This flow equation yields a well-defined solution as $k \to 0$, as long as the regulator is masslike [53,54], i.e., $R_{k>0}(0) > 0$. Furthermore, it functionally mimics a zero-dimensional RG flow, which must lead to a strictly convex quantum effective action in the IR limit, see Refs. [55–59]. This is in accordance with the general absence of spontaneous symmetry breaking on finite spacetime lattices.

Note that due to the evaluation of the propagator (27) at $\boldsymbol{q} = \boldsymbol{0}$, the flow equation for the scale-dependent effective potential completely decouples from the nontrivial kinetic structure $\Delta\bar{\Gamma}^{(2)}_k$. Meaning that, in the IR regime, the scale-dependent effective potential is not affected by couplings like a wave-function renormalization or other couplings associated with the momentum structure of the scale-dependent effective action.

Finally, note that the assumption of translational invariance, used in Eq. (26), is almost always inherent in the truncation ansatz employed in fRG studies.

2. Ultraviolet regime

Let us now discuss the UV regime of the RG flow. Specifically, we focus on this regime for regulators to which we refer as lattice site decoupling regulators. These are regulators which, above a certain RG scale $k^\star$—the lattice site decoupling scale—eliminate any kinetic structure in the propagator. As a result, the scale-dependent partition function $\mathcal{Z}_k[J]$ in Eq. (19) reduces to a product of zero-dimensional partition functions $\mathcal{Z}^{0d}_k(J_{\boldsymbol{x}})$. Meaning that the regulator term in the action renders all fluctuations purely local in this regime, see Ref. [36].

More precisely, in order to qualify as lattice site decoupling, the regulator must fulfill

$$R_{k>k^\star}(\epsilon_{\boldsymbol{q}}) = M^2_k - \epsilon^2_{\boldsymbol{q}}, \tag{34}$$

for all RG scales k greater than the decoupling scale $k^\star$, which implies that

$$S[\phi] + \Delta S_{k>k^\star}[\phi] = a^d \sum_{\boldsymbol{x}\in\mathcal{V}} \frac{M^2_k}{2}\phi^2_{\boldsymbol{x}} + a^d \sum_{\boldsymbol{x}\in\mathcal{V}} \mathcal{U}(\phi_{\boldsymbol{x}}) \tag{35}$$

is a purely local action. Here, M_k is a k-dependent mass term to be chosen such that it diverges as $k \to \infty$. This property guarantees that the scale-dependent effective average action $\bar{\Gamma}_k$ approaches the bare action S in the UV limit, as we shall show below. For example, the Litim

regulator (23) with $k^\star = \epsilon_{\max}$ and $M_k = k$ is of this type.[5] For the scale-dependent partition function (19) we find

$$\mathcal{Z}_{k>k^\star}[J] = \int \mathcal{D}\phi \prod_{x\in\mathcal{V}} e^{-a^d(\frac{1}{2}M_k^2\phi_x^2 + \mathcal{U}(\phi_x) - J_x\phi_x)} = \prod_{x\in\mathcal{V}} \mathcal{Z}_k^{0d}(a^d J_x), \tag{36}$$

where we have used Eq. (2) and introduced the zero-dimensional partition function

$$\mathcal{Z}_k^{0d}(j) = a^{d_\phi}\int_{-\infty}^{\infty} \mathrm{d}\varphi e^{-S_k^{0d}(\varphi)+j\varphi}, \tag{37}$$

with $S_k^{0d}(\varphi) = a^d(\frac{1}{2}M_k^2\varphi^2 + \mathcal{U}(\varphi))$. For the Schwinger functional we analogously find

$$W_{k>k^\star}[J] = \sum_{x\in\mathcal{V}} W_k^{0d}(a^d J_x), \tag{38}$$

where $W_k^{0d}(j) = \ln \mathcal{Z}_k^{0d}(j)$. Due to the simple structure of Eq. (38), we find

$$a^{-d}\frac{\partial}{\partial J_x} W_{k>k^\star}[J] = W_k^{0d(1)}(a^d J_x). \tag{39}$$

This implies that $J_x[\phi] = a^{-d}[W_k^{0d(1)}]^{-1}(\phi_x)$. Hence, the Legendre transform of $W_k[J]$, i.e., the scale-dependent effective action, reads

$$\begin{aligned}\Gamma_{k>k^\star}[\phi] &= a^d\sum_{x\in\mathcal{V}} J_x[\phi]\phi_x - W_{k>k^\star}[J[\phi]] \\ &= \sum_{x\in\mathcal{V}}\left([W_k^{0d(1)}]^{-1}(\phi_x)\phi_x - W_k^{0d}([W_k^{0d(1)}]^{-1}(\phi_x))\right) \\ &= \sum_{x\in\mathcal{V}}\Gamma_k^{0d}(\phi_x).\end{aligned} \tag{40}$$

The modified Legendre transform, the scale-dependent effective average action, is then given by

$$\begin{aligned}\bar{\Gamma}_{k>k^\star}[\phi] &= \sum_{x\in\mathcal{V}}\Gamma_k^{0d}(\phi_x) - \Delta S_k[\phi] \\ &= \frac{1}{V}\sum_{q\in\tilde{\mathcal{V}}}\frac{\epsilon_q^2}{2}\tilde{\phi}_{-q}\tilde{\phi}_q + \sum_{x\in\mathcal{V}}\left(\Gamma_k^{0d}(\phi_x) - a^d\frac{M_k^2}{2}\phi_x^2\right).\end{aligned} \tag{41}$$

It is worth mentioning that, due to the regulator term $\Delta S_k[\phi]$ in the modified Legendre transformation in Eq. (41), a kinetic contribution is added to the scale-dependent effective average action. Furthermore, since we did not yet make any approximation, the solution (41) is exact which means that it is a solution of the (untruncated) Wetterich equation (20) for $k > k^\star$. Only the term associated with the potential in $\bar{\Gamma}_k$ changes during the RG flow, other couplings are *not* generated. This reflects the purely local structure of the theory for RG scales $k > k^\star$. From this analysis, we conclude that the use of a lattice site decoupling regulator is advisable in actual applications of our lattice fRG framework.

Finally, using Eq. (41), we can prove that the scale-dependent effective average action indeed approaches the bare action S as $k \to \infty$. To this end, we note that $[W_k^{0d(1)}]^{-1}(\phi_x) \sim a^d M_k^2\phi_x$ as $k\to\infty$ which implies

$$\begin{aligned}&\Gamma_k^{0d}(\phi_x) - a^d\frac{M_k^2}{2}\phi_x^2 \\ &\quad = -\ln\left(a^{d_\phi}\int_{-\infty}^{\infty}\mathrm{d}\varphi e^{-a^d\mathcal{U}(\varphi)}e^{-a^d\frac{M_k^2}{2}(\varphi-\phi_x)^2}\right) \\ &\quad \sim a^d\mathcal{U}(\phi_x) + C\end{aligned} \tag{42}$$

for $k\to\infty$. Here, C is a field independent and thus irrelevant constant. We would like to stress that each term in Eq. (42) diverges separately. However, the combination of all terms yields the finite bare potential in the UV limit and thus $\bar{\Gamma}_k[\phi] \to S[\phi]$ as $k\to\infty$. Note that this also implies the UV behavior of the couplings as shown in Eq. (22).

3. Intermediate regime

In the intermediate regime, $\Delta\epsilon \le k \le \epsilon_{\max}$, the RG flow is nontrivial and in principle all couplings allowed by the symmetries of a given model are dynamically generated. We add that the size of this regime shrinks as we decrease the number of lattice sites N_σ and disappears for $N_\sigma = 1$.

B. Local potential approximation

As we have already seen in Secs. IV A 1 and IV A 2, the effective potential in the scale-dependent effective average action plays a dominant role in the IR as well as in the UV regime, especially in case of regulators satisfying the properties (30) and (34). To describe these regimes accurately, it is therefore mandatory to consider an approximation of the Wetterich equation (20) which is exact in these limits. This is the case for the LPA as these limits correspond to zero-dimensional theories. In the following we shall therefore employ this approximation which represents the lowest order of the derivative expansion but already goes beyond the mean-field approximation as it takes into account fluctuation effects.

The LPA assumes in every RG step the ansatz

$$\bar{\Gamma}_k[\phi] = \frac{1}{V}\sum_{q\in\tilde{\mathcal{V}}}\frac{\epsilon_q^2}{2}\tilde{\phi}_{-q}\tilde{\phi}_q + a^d\sum_{x\in\mathcal{V}} U_k(\phi_x) \tag{43}$$

[5]Another example for a lattice site decoupling regulator is the smooth Litim regulator introduced in Ref. [60] which has $k^\star = \sqrt{2}\epsilon_{\max}$ as its lattice site decoupling scale.

for the scale-dependent effective average action on the right-hand side of the Wetterich equation (20). This implies that terms associated with derivatives of the fields enter the right-hand side of the Wetterich equation only in the form as they appear in the classical action. Nevertheless, within LPA, such couplings are dynamically generated, especially in the aforementioned intermediate regime of the RG flow and can in principle be straightforwardly calculated by taking field derivatives on both sides of the Wetterich equation (24).

Using Eq. (43) as truncation for the scale-dependent effective action, the kinetic contribution is simply given by $\Delta\bar{\Gamma}_k^{(2)}(\varphi, \boldsymbol{q}) = \epsilon_{\boldsymbol{q}}^2$, and thus the propagator (27) reads

$$G_k^{(2)}(\varphi, \boldsymbol{q}) = \frac{1}{\partial_\varphi^2 U_k(\varphi) + \epsilon_{\boldsymbol{q}}^2 + R_k(\epsilon_{\boldsymbol{q}})}. \tag{44}$$

In particular, for the Litim regulator (23), we have $\epsilon_{\boldsymbol{q}}^2 + R_k(\epsilon_{\boldsymbol{q}}) = k^2$ for $k \leq \epsilon_{\boldsymbol{q}}$. Hence, evaluating the Wetterich equation (24) at a constant background field configuration, $\boldsymbol{\phi} = (\varphi, \ldots, \varphi)$, and using the Litim regulator, the flow equation for the scale-dependent effective potential reads

$$\partial_t U_k(\varphi) = \frac{1}{2}\Omega(k)\frac{\partial_t k^2}{k^2 + \partial_\varphi^2 U_k(\varphi)}, \tag{45}$$

where $\Omega(k)$ is the density of modes,

$$\Omega(k) = \frac{1}{V}\sum_{\boldsymbol{q}\in\tilde{\mathcal{V}}}\Theta(k^2 - \epsilon_{\boldsymbol{q}}^2). \tag{46}$$

In the UV regime, $k > \epsilon_{\max}$, we find $\Omega(k) = a^{-d}$. In the IR regime, $k < \Delta\epsilon$, we have $\Omega(k) = 1/V$.[6] We emphasize that, even in this approximation, the flow equation (45) already represents a highly nonlinear diffusion equation. In Appendix A, we discuss the numerical setup used to solve this differential equation in the present work.

In Fig. 1, we illustrate the behavior of various quantities in the RG flow for the bare action (3) in $d = 3$ dimensions with $a\lambda = 6$ and $(am)^2 = -1$. To be specific, we show the scale-dependent (global) minimum $\varphi_0(k)$ of the scale-dependent potential U_k, the curvature mass $m(k)$ evaluated at $\varphi_0(k)$ of U_k, and the density of modes $\Omega(k)$ as functions of the RG scale k. We observe that $\varphi_0(k)$ and $m(k)$ approach plateaus, reflecting the convergence of $U_k \to \mathcal{U}$ in the UV limit, i.e., as $k \to \infty$. From this figure we also

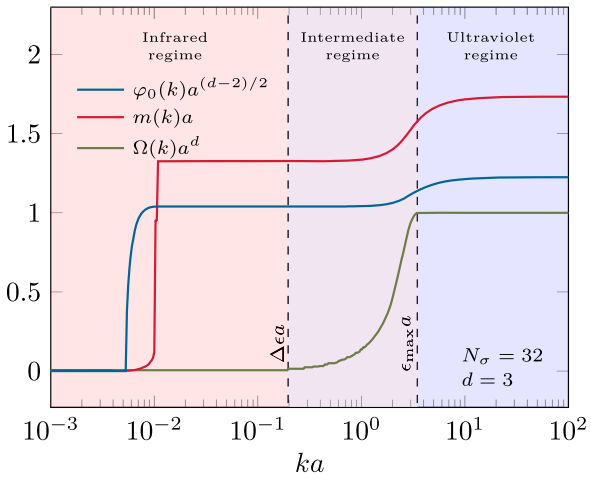

FIG. 1. Illustration of the RG flow of the (global) minimum $\varphi_0(k)$ of the potential U_k, the curvature mass $m(k)$ evaluated at the minimum $\varphi_0(k)$ of U_k, and the density of modes $\Omega(k)$ in the IR, intermediate, and UV regimes for a given bare action, see main text for details.

deduce that, for a given bare action, it is indeed possible to find a finite initial RG scale that is sufficiently large to suppress artifacts associated with its finiteness. For the specific parameter set represented in Fig. 1, we find that $\Lambda = 100/a$ is sufficiently large. We add that the RG flow is exact down to the lattice site decoupling scale $k^\star = \epsilon_{\max}$, as discussed in Sec. IV A 2. The density of modes $\Omega(k)$ remains constant in this regime.

In the intermediate regime, the RG flow in LPA is no longer exact. Here, the mode density decreases as the RG scale is lowered until it reaches $\Omega(k = \Delta\epsilon) = 1/V$. The corresponding scale defines the onset of the IR regime. In this regime, the flow equation for the scale-dependent effective potential completely decouples from kinetic contributions and only the zero mode contributes to the RG flow, see Eq. (32). The LPA is then no longer an approximation but exact again. As a consequence of the fact that the RG flow reduces to that of a zero-dimensional system in this regime, the minimum $\varphi_0(k)$ eventually approaches zero for $k \to 0$. Thus, there is no spontaneous symmetry breaking in the IR limit, as it should be for zero-dimensional systems. The curvature mass $m(k)$ approaches a small positive value, indicating the formation of a very flat but strictly convex effective potential in the IR limit. Note that the flow equation associated with this regime, which can be extracted from Eq. (45) by replacing the mode density with $1/V$, is indeed reminiscent of that of a zero-dimensional system, see also Sec. IV A 1.

V. RESULTS

We begin the discussion of our numerical results by noting that we shall choose $\lambda a^{4-d} = 6$ for the quartic coupling for all spacetime dimensions d considered in this

[6]For comparison, in a continuous and infinite spacetime, we find

$$\Omega(k) = \frac{\mathrm{surf}(d)}{(2\pi)^d}\frac{1}{d}k^d,$$

where $\mathrm{surf}(d)$ is the surface of a d-dimensional unit sphere.

work. Thus, with respect to the parameters of our model, we vary only the squared bare mass parameter m^2 and the external field c, which is sufficient for a study of SSB and phase transitions. All dimensionful quantities shall be given in units of the lattice spacing a. For notational convenience, we are using natural units, "$a = 1$", from here on.

A. FRG: Assessing LPA

To obtain an intrinsic check of the reliability of LPA, we analyze the kinetic term in the propagator (27). To that end, we derive the flow equation for the quantity $\Delta\bar{\Gamma}_k^{(2)}(\varphi, \boldsymbol{p})$ defined in Eq. (29). This is done by first taking two field derivatives on both sides of the Wetterich equation (24) and evaluating the resulting flow equation on a constant background field configuration $\boldsymbol{\phi} = (\varphi, \ldots, \varphi)$. From this, we then obtain the following expression in LPA:

$$\partial_t \Delta\bar{\Gamma}_k^{(2)}(\varphi, \boldsymbol{p}) = \frac{1}{V}\sum_{\boldsymbol{q}\in\tilde{\mathcal{V}}} \partial_t R_k(\epsilon_{\boldsymbol{q}}) \Big(G_k^{(2)}(\varphi, \boldsymbol{q})\partial_\varphi^3 U_k(\varphi)\Big)^2 \times \Big[G_k^{(2)}(\varphi, \boldsymbol{q}-\boldsymbol{p}) - G_k^{(2)}(\varphi, \boldsymbol{q})\Big]. \tag{47}$$

The definition of the propagator $G_k^{(2)}$ can be found in Eq. (44). Since the propagators on the right-hand side of Eq. (47) do not depend on $\Delta\bar{\Gamma}_k^{(2)}$ itself (as we work in LPA), this flow equation is not a coupled differential equation and can therefore be integrated straightforwardly by inserting the solution for the effective potential U_k from Eq. (45) for a given set of parameters.

We emphasize that, for RG scales above the lattice site decoupling scale $k^\star$ (i.e., in the UV regime), the propagator $G_k^{(2)}(\varphi, \boldsymbol{q})$ becomes independent of the momenta and therefore the difference of the two propagators on the right-hand side of Eq. (47) vanishes identically. In this regime, the kinetic term does not receive any quantum corrections in the RG flow. This again reflects the exactness of LPA at these scales, as discussed in Sec. IV A 2.

Equation (47) can be used to estimate the uncertainty of LPA in the intermediate regime where this approximation is not exact. To be more specific, if we would find that the change of the momentum-dependent part of the two-point function relative to its classical form is exactly zero or at least very small for all momenta and field values, then LPA can be expected to be a reasonable approximation for a determination of the effective potential. To quantify the uncertainty of LPA, we therefore define

$$\mathcal{K}(\boldsymbol{q}) = \max_{\varphi\geq\varphi_0(k=\epsilon_{\boldsymbol{q}})} \left|\frac{\Delta\bar{\Gamma}_{k=\epsilon_{\boldsymbol{q}}}^{(2)}(\varphi, \boldsymbol{q}) - \epsilon_{\boldsymbol{q}}^2}{\epsilon_{\boldsymbol{q}}^2}\right|. \tag{48}$$

This quantity represents the maximum relative deviation of the momentum-dependent part of the two-point function, as obtained in an LPA flow for a given momentum $\boldsymbol{q}$, from the momentum dependence assumed in LPA. The latter is nothing but the classical kinetic term. Note that, in Eq. (48), we only take field values inside the physically relevant region into account, i.e., for $\varphi \geq \varphi_0(k)$. In the physically irrelevant region, i.e., for field values $\varphi < \varphi_0(k)$, the momentum-dependent part of the two-point function drastically changes since the potential becomes flat there. This would strongly dominate the relative deviation $\mathcal{K}$.

Because of the property (30) of the Litim regulator, only momentum-dependent contributions $\Delta\bar{\Gamma}_k^{(2)}(\varphi, \boldsymbol{q})$ with $\epsilon_{\boldsymbol{q}} < k$ are required to determine the next RG step for the scale-dependent effective potential U_k, see Eq. (31). In other words, the evolution of the scale-dependent effective potential U_k for $k \to 0$ is not directly affected by the parts of $\Delta\bar{\Gamma}_k^{(2)}(\varphi, \boldsymbol{q})$ with $\epsilon_{\boldsymbol{q}} > k$. This is also reflected in the decrease of the mode density $\Omega(k)$ as the IR limit is approached, see Fig. 1. Therefore, to include only the regime of the RG flow which affects the flow equation for the scale-dependent effective potential for a certain momentum $\boldsymbol{q}$ in Eq. (48), we evaluate $\Delta\bar{\Gamma}_k^{(2)}(\varphi, \boldsymbol{q})$ at $k = \epsilon_{\boldsymbol{q}}$.

It is important to emphasize that the quantity defined in Eq. (48) serves solely as a measure to *estimate* the uncertainty of LPA. It should be interpreted as follows: If the value of $\mathcal{K}(\boldsymbol{q})$ is small, LPA can be considered as a reliable approximation whereas no definitive statement can be made about the validity of LPA for large $\mathcal{K}(\boldsymbol{q})$.

Since the RG evolution of the two-point function depends on the solution for the effective potential U_k and, consequently, on the parameters that determine the bare action, namely m^2 and λ, we analyze the relative deviation (48) as a function of m^2 while keeping $\lambda = 6$ fixed. In Fig. 2, we show the relative deviation (48) evaluated on the mode associated with the lowest nonzero energy level $\Delta\epsilon$ for one-, two-, and three-dimensional systems with $N_\sigma = 16, 32, 64$ lattice sites in each direction. Note that the modes associated with $\Delta\epsilon$ are the only modes which remain "active" in the RG flow down to the IR regime and can therefore significantly influence the evolution of the scale-dependent effective potential throughout the entire intermediate regime.

We observe that the relative deviation is generally smaller for $d = 3$ than for $d = 2$ spacetime dimensions. This is in accordance with the general observation that the anomalous dimension at a critical fixed point increases in scalar field theories when the number of spacetime dimensions is decreased, see, e.g., Ref. [61] for a review.[7] For example, the anomalous dimension at such a fixed point in $d = 3$ is about one order of magnitude smaller than in

[7] In our setting, the anomalous dimension η can be defined in terms of the exponential decay of the propagator at criticality for $N_\sigma \to \infty$, i.e., $G_{k=0}^{(2)}(\varphi = 0, \boldsymbol{q}_0) \sim \epsilon_{\boldsymbol{q}_0}^{-1+\eta/2} a^{-\eta}$ for $N_\sigma \to \infty$. Here, $\boldsymbol{q}_0$ is a momentum mode with $\epsilon_{\boldsymbol{q}_0} \equiv \Delta\epsilon$ where $\Delta\epsilon$ is the lowest nonzero kinetic energy level, see Sec. IV A.

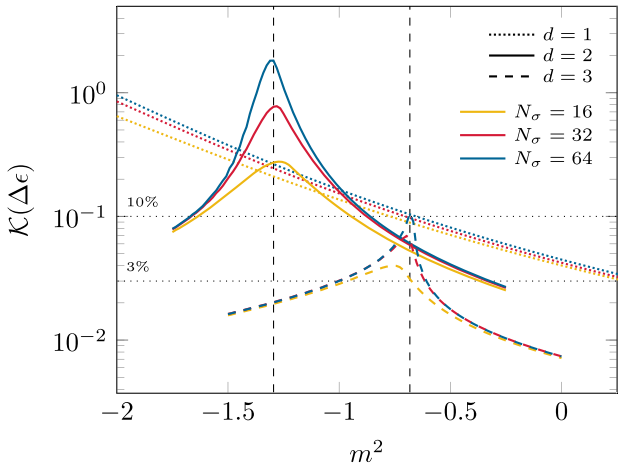

FIG. 2. The relative deviation of the fluctuation-induced kinetic term (48) from its classical form as a function of the bare mass m^2.

$d = 2$. Moreover, this observation with respect to the relative deviation is consistent with the fact that the critical exponents obtained in LPA in $d = 3$, where $\eta = 0$ by construction, already agree on the percent level with the world's best estimates, see, e.g., Refs. [61–66]. At least close to a phase transition, a large anomalous dimension can therefore be considered an indication for the formation of a nontrivial momentum dependence of the two-point function. In any case, in both $d = 2$ and $d = 3$, we observe peaklike structures that become sharper as N_σ increases. For $N_\sigma = 64$, the positions of these peaks are located at $m^2_{\text{peak}} \approx -1.295$ and $m^2_{\text{peak}} \approx -0.682$ for $d = 2$ and $d = 3$, respectively. As we shall see below, these peaklike structures emerge close to the phase transition. For better guidance of the eye, we included horizontal lines in Fig. 2 to indicate the regions in the m^2-plane where the relative deviation $\mathcal{K}$ evaluated on the lowest nontrivial mode $\Delta\epsilon$ is above 3% and 10%, respectively. The precise values for the boundaries of these regions are listed in Table I for $N_\sigma = 64$.

For completeness, we also show the scale-dependent global minimum $\varphi_0(k)$ as well as the scale-dependent correlation length $\xi(k) = 1/m(k)$ evaluated at the RG scale $k = \Delta\epsilon$ as functions of m^2 in Fig. 3. Note that, since we evaluated these quantities at a nonzero RG scale, the effective potential $U_{k=\Delta\epsilon}$ need not be convex and the $Z(2)$ symmetry in the ground state is not yet necessarily restored at this scale. This explains the regions with a finite value of φ_0 in Fig. 3(a). The vertical dashed lines in both panels of Fig. 3 indicate the position of the peaks in the relative deviation $\mathcal{K}$ for $N_\sigma = 64$ in $d = 2$ and $d = 3$ spacetime dimensions, respectively, see Fig. 2. Note that the peaks in the relative deviation do not coincide exactly with those of the correlation length, but approach each other as the spatial volume is increased. This is a finite-size effect that will disappear in the thermodynamic limit, where a nonanalytic phase transition emerges, and indicates that the two-point function develops a nontrivial momentum dependence close to the phase transition.

TABLE I. List of characteristic quantities of $\mathcal{K}(\Delta\epsilon)$, i.e., the relative deviation of the fluctuation-induced kinetic term from its classical form, as extracted from Fig. 2 for $N_\sigma = 64$.

d	N_σ	$\mathcal{K}(\Delta\epsilon) \geq 10\%$	$\mathcal{K}(\Delta\epsilon) \geq 3\%$	m^2_{peak}
2	64	$m^2 \in [-1.659, -0.871]$	$m^2 \in [-1.75, -0.325]$	−1.295
3	64	$m^2 \in \{-0.682\}$	$m^2 \in [-1.0, -0.810]$	−0.682

In Fig. 2, we also show the relative deviation for $d = 1$ spacetime dimensions. The corresponding partition function can be associated with the anharmonic oscillator in quantum mechanics. In this case, the curvature of the effective potential U at its minimum is related to the energy difference between the two lowest levels of the system. Although the symmetry in the ground state is found to be restored in LPA, as it should be, it has already been shown by comparison with exact results in Ref. [67] that LPA does not provide quantitative results for the energy difference of the two lowest-lying states for small values of the dimensionless coupling $\lambda/|m^2|^{3/2}$ with $m^2 < 0$ and $\lambda > 0$. This implies that LPA does not allow one to correctly recover the effective potential for classical potentials with a large potential barrier in $d = 1$. This can be traced back to the relevance of instanton effects, which are not included in our current LPA calculation [67]. For sufficiently large values of the dimensionless coupling, LPA yields results for the difference of the two lowest-lying energy levels which are in quantitative agreement with the exact results. Note that this observation is in accordance with the behavior of the relative deviation (48) in Fig. 2. Indeed, we observe that the relative deviation $\mathcal{K}$ increases as m^2 is lowered for $d = 1$. This can be understood as follows: As we approach the limit of an infinitely negative value of m^2, the effective potential becomes arbitrarily flat and the correlation length increases accordingly, see Fig. 3(b). Note also that the nontrivial minimum $\varphi_0(\Delta\epsilon)$ of U must vanish for large enough volumes due to the Mermin-Wagner theorem. As a consequence, *all* field values contribute to the relative deviation $\mathcal{K}$ as defined in Eq. (48), including those where the effective potential is very flat.

Finally, we would like to emphasize that all quantities shown in Figs. 2 and 3 carry an intrinsic dependence on the regulator R_k, irrespective of the fact that we did not solve the Wetterich equation exactly. In fact, these quantities have been extracted from the RG flow at a nonzero RG scale k which inherently depends on the choice of regulator. Note also that we choose $k = \Delta\epsilon$ since our regulator fulfills the property (30). This renders the flow equation for the scale-dependent effective potential (33) exact for $k < \Delta\epsilon$ which is only the case for a specific class of regulators.

In summary, we have defined an fRG-intrinsic measure, the relative deviation of the momentum-dependent part of

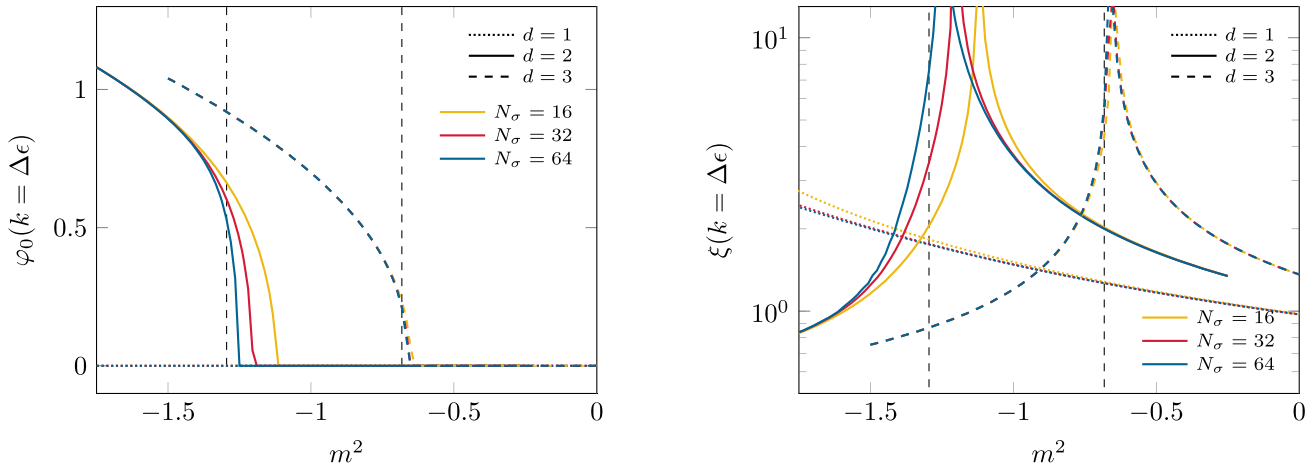

(a) Magnetization. (b) Correlation length.

FIG. 3. Global minimum $\varphi_0(k)$ of the effective potential (a) and correlation length $\xi(k)=1/m(k)$ (b) evaluated at the RG scale $k=\Delta\epsilon$ for a fixed bare coupling $\lambda=6$ as functions of the bare mass m^2 as obtained for different lattices sizes N_σ in $d=2$ and $d=3$ dimensions, respectively. Vertical lines mark the peak of the susceptibility on $N_\sigma=64$.

the two-point function from its classical counterpart, which allows us to estimate the uncertainty of LPA in different regimes, see Eq. (48). Our analysis based on this measure indicates that LPA tends to be more reliable the smaller the spacetime lattices, the higher the spacetime dimensions, and sufficiently far away from the critical regime. However, we stress that this criterion does not determine how a given relative deviation in the momentum-dependent part of the two-point function affects other physical observables. This question must be addressed by comparing our LPA results with those obtained using the MC approach.

B. Comparison of lattice MC and lattice fRG

The present work aims at a quantitative comparison of two nonperturbative methods, lattice MC and lattice fRG, rather than at a study of phenomenological aspects of spin models. For this comparison, we perform calculations over a wide range of the model parameters m and c while keeping the quartic coupling λ fixed.

In addition to our fRG-intrinsic analysis of the predictive power of LPA in the previous subsection, a comparison of our lattice fRG and lattice MC results allows us to examine and quantify the limitations of LPA in more detail.

1. Effective potential

In the fRG approach we have direct access to the effective potential as it is the solution of the flow equation (45) in the IR limit. For a lattice MC computation of this potential, one may exploit the identity (13), i.e.,

$$\partial_\varphi U(\langle M\rangle_{V,c}) = c.$$

This equation relates the magnetization with the effective potential and can be used to obtain the latter by performing MC calculations for different values of c. To be specific, by computing $\langle M\rangle_{V,c}$ as a function of c and assuming that this relation can be inverted, we find $c=c(\langle M\rangle_{V,c})$. The effective potential in the absence of an external field can then be obtained as follows:

$$U(\varphi) = \int_{\bar\varphi}^{\varphi} \mathrm{d}\varphi' c(\varphi') + \text{const.}, \tag{49}$$

where we have used (13) and the lower integration boundary is given by $\bar\varphi = \lim_{c\to 0}\langle M\rangle_{V,c}$.

We emphasize that the effective potential is analytic and strictly convex in finite systems. In the thermodynamic limit, this is still the case in the absence of SSB, where we have $\bar\varphi=0$. However, if the ground state is governed by SSB, then the effective potential becomes nonanalytic at $\varphi=\bar\varphi=\lim_{c\to 0}\langle M\rangle_{V,c}$ and we have $\partial_\varphi U(\varphi)=0$ for $\varphi<\bar\varphi$, i.e., the effective potential is flat within this range of field values. These considerations imply that we can already analyze the shape of the effective potential by studying the dependence of the magnetization on c. In particular, in our studies of finite systems, where the effective potential is analytic, the c dependence of the magnetization and its susceptibility can be employed to detect regions in parameter space where the effective potential becomes flat over a finite range of field values, indicating SSB in the thermodynamic limit. Recall that the susceptibility is determined by the inverse of the curvature of the effective potential, see Eq. (16). For example, a rapid increase in the susceptibility for small values of the external field c indicates the formation of a nonanalyticity in the effective potential and the formation of a flat regime. We shall discuss this in more detail below.

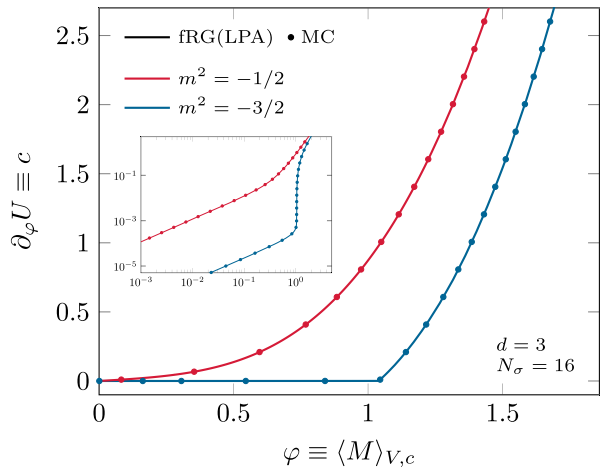

FIG. 4. Field derivative of the effective potential U as a function of the field for $m^2 = -1/2$ and $m^2 = -3/2$ in three spacetime dimensions with $N_\sigma = 16$.

For illustration, we show the field derivative of the effective potential for $m^2 = -3/2$ and $m^2 = -1/2$ in $d = 3$ spacetime dimensions for $N_\sigma = 16$ as a function of the magnetization in Fig. 4. These results imply that the associated effective potential is strictly convex in both cases and has a global minimum at $\varphi = 0$, reflecting the absence of SSB in finite systems. For $m^2 = -3/2$, however, our results for the field derivative of the effective potential indicate that the effective potential itself is already very flat in the region $0 \leq \varphi \lesssim 1$. From Fig. 4, we can also deduce that the curvature of the effective potential undergoes a rapid change at the point where the potential becomes flat. This translates into a rapid change of the susceptibility $\sim \partial \langle M \rangle_{V,c} / \partial c$ as a function of the external field c, as we shall see below. Following our discussion above, this behavior of the field derivative of the effective potential for $m^2 = -3/2$ can be considered a precursor for the formation of a phase with a finite magnetization in the thermodynamic limit. For $m^2 = -1/2$, the situation is different. Indeed, we do not find that the potential develops a flat region in field space. Therefore, we expect the system to remain in the $Z(2)$-symmetric phase in the thermodynamic limit. In any case, for both values of m^2, we find that the effective potential from our lattice fRG study in LPA agrees remarkably well with the results from our MC calculations.

2. Precursors of SSB in finite systems

Without explicitly considering the thermodynamic limit, we can already deduce from the behavior of the effective potential under a variation of N_σ (for a fixed lattice spacing) whether the ground state is governed by SSB in the thermodynamic limit. As mentioned above, the behavior of the effective potential is also encoded in the magnetization as a function of the external field c. To be specific, coming from large values of the external field c, SSB manifests itself as the formation of a plateau in the magnetization as c is decreased. For a system with a given set of model parameters in d spacetime dimensions, we shall see that this plateau increases with increasing N_σ and eventually extends to $c = 0$, if the ground state is governed by SSB in the thermodynamic limit. The formation of such a plateau can therefore be regarded as a precursor of SSB in finite systems. Of course, whether this plateau extends to $c = 0$ for $N_\sigma \to \infty$ and thus truly indicates SSB in the thermodynamic limit must always be analyzed by studying the scaling of the magnetization with N_σ. We add that, in the presence of SSB in the thermodynamic limit, the disappearance of the magnetization in a finite system for $c \to 0$ is a finite-volume effect.

Let us now compare our results for the magnetization and the susceptibility in different spacetime dimensions as obtained by our two nonperturbative approaches.

One dimension. For $m^2 > 0$, this system corresponds to the anharmonic oscillator in quantum mechanics. The case with $m^2 < 0$, which we consider from here on, is a model to study tunneling in quantum mechanics. In any case, the relation to quantum-mechanical one-particle systems already indicates that SSB cannot occur in $d = 1$, which we also find in our present study. Note that this is correct regardless of our choice of model parameter values. Accordingly, the magnetization in one dimension must vanish when we consider the limit $c \to 0$ after the limit $N_\sigma \to \infty$ has been taken.

In Fig. 5, we show the magnetization and the susceptibility as a function of c for various values of N_σ and two values for $m^2 < 0$. As explained above, the quartic coupling has been set to the same value $\lambda = 6$ in the two cases. For all considered values of N_σ and m^2, we do not observe the formation of a plateau in the magnetization as a function of the external field c. In fact, the magnetization tends to zero as we decrease c while the susceptibility remains finite. Moreover, in accordance with our fRG-intrinsic analysis of the reliability of LPA in Sec. V A, we find that the deviation of our lattice fRG results from the lattice MC results increases with decreasing m^2. This can be traced back to the fact that an accurate resolution of the momentum dependence of the correlation functions becomes very relevant for a quantitatively correct description of tunneling through a (high) potential barrier. In any case, while inaccurate on a quantitative level for increasing N_σ, the disappearance of the magnetization for $c \to 0$ in the thermodynamic limit is still observed in LPA.

We close the discussion of the one-dimensional case by adding that the lattice MC and lattice fRG results are overall in excellent agreement for small values of N_σ. This is true regardless of the dimension of the system, see also below. Of course, this does not come unexpected as LPA becomes exact for $N_\sigma = 1$ which corresponds to the case of a zero-dimensional quantum field theory [56–59].

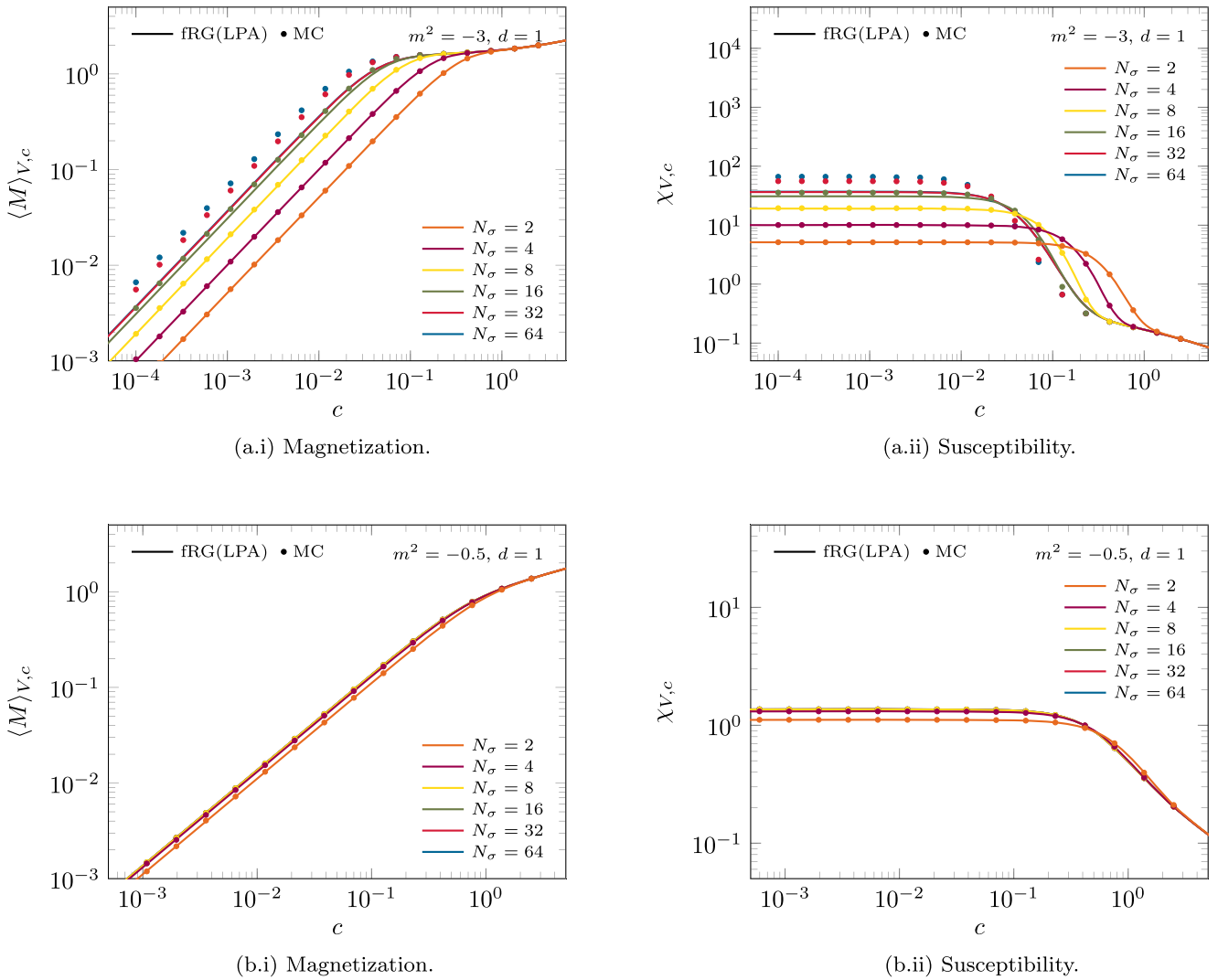

(a.i) Magnetization. (a.ii) Susceptibility.

(b.i) Magnetization. (b.ii) Susceptibility.

FIG. 5. Magnetization and susceptibility in one spacetime dimension as a function of the external field c, as obtained from lattice MC (dots) and lattice fRG (solid lines) calculations, in panels (a.i) and (a.ii) for $m^2 = -3$, and in panels (b.i) and (b.ii) for $m^2 = -0.5$.

Two dimensions. In Fig. 6, the magnetization and the susceptibility are shown as functions of the external field c for $m^2 = -1.5$ and $m^2 = -0.5$ as obtained for various values of N_σ in two spacetime dimensions. The quartic coupling is the same in both cases. We readily observe that the lattice MC and lattice fRG results for the magnetization are in good agreement. The two values selected for the parameter m^2 are associated with qualitatively different situations in the thermodynamic limit, as we shall see next.

For $m^2 = -1.5$, we observe the formation of a plateau in the magnetization as a function of the external field c, which becomes broader continuously as we increase N_σ. Thus, for this value of m^2 we expect the system to be in the symmetry broken phase where the ground state is governed by spontaneous $Z(2)$ symmetry breaking in the thermodynamic limit for $c \to 0$. Our results make apparent that the order of the limits $c \to 0$ and $N_\sigma \to \infty$ do not commute. In fact, to obtain a finite magnetization in the thermodynamic limit, we have to take the limit $c \to 0$ *after* the thermodynamic limit, $N_\sigma \to \infty$, see also Eq. (7).

For $m^2 = -0.5$, we do not observe the formation of a plateau in the magnetization, even for large values of N_σ. For increasing N_σ, we rather find that the results from both methods converge to a continuous function which tends to zero for $c \to 0$. Consequently, we expect the system to be in the symmetric phase in the thermodynamic limit for this value of m^2.

Let us now consider the susceptibility, which is a more sensitive probe for the detection of differences between our lattice fRG and the lattice MC results, since it corresponds to the derivative of the magnetization with respect to the external field c and measures fluctuations. Still, we observe that the results for the susceptibility agree well for $m^2 = -0.5$. However, deviations are found for $m^2 = -1.5$ as N_σ increases. Note that, for this value of m^2, the system is in the symmetry broken phase but still not far

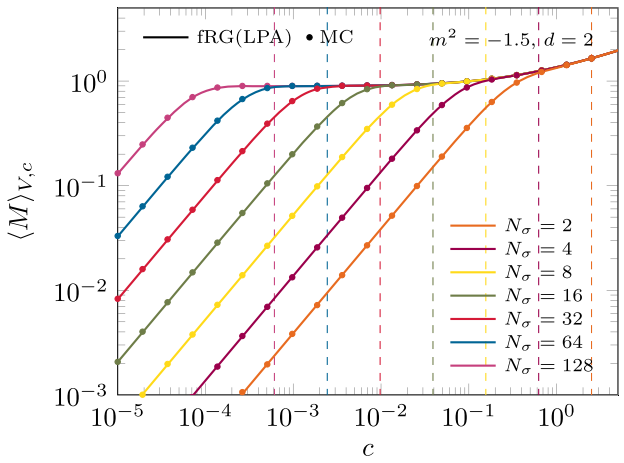

(a.i) Magnetization.

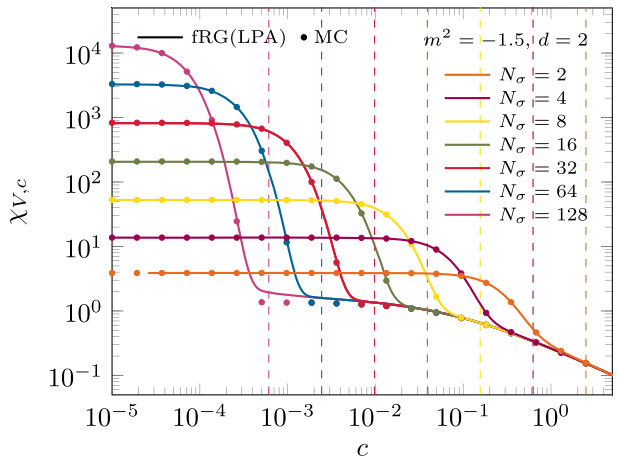

(a.ii) Susceptibility.

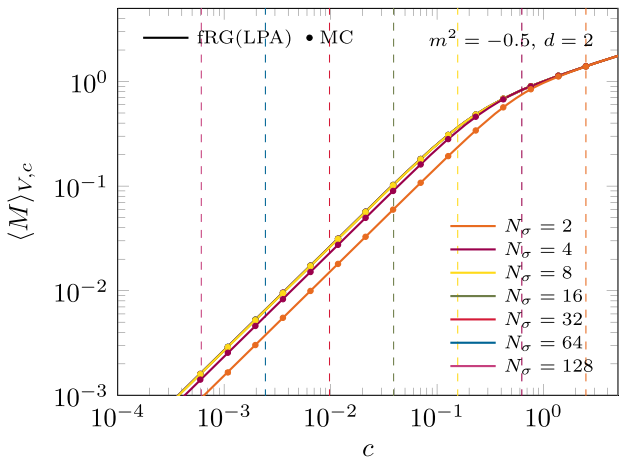

(b.i) Magnetization.

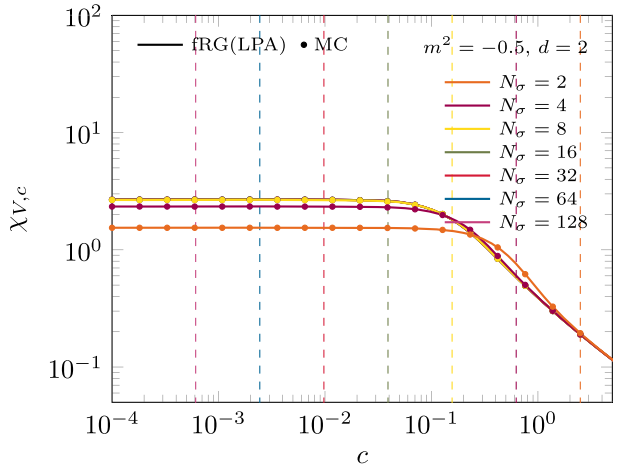

(b.ii) Susceptibility.

FIG. 6. Magnetization and susceptibility in two spacetime dimensions as a function of the external field c, as obtained from lattice MC (dots) and lattice fRG (solid lines) calculations, in panels (a.i) and (a.ii) for $m^2 = -1.5$, and in panels (b.i) and (b.ii) for $m^2 = -0.5$. The vertical dashed lines indicate the values of c at which the magnetization and susceptibility for the corresponding values of m^2 and N_σ have been extracted for our analysis of the m^2 dependence of these quantities in Fig. 8, see main text for details.

away from the phase transition in m^2, see our discussion of phase transitions below. Since our lattice fRG calculations are based on LPA, these deviations of the lattice fRG results from the lattice MC results already hint at the importance of a nontrivial momentum dependence in the correlation functions, which become increasingly relevant close to the phase transition. We shall come back to this aspect below, as we would first like to discuss characteristic features of the susceptibility in finite systems.

In our results for the susceptibility in the symmetry broken phase approaching the thermodynamic limit, we observe the formation of two plateaus, one appearing for very small values of c and the other for small but not too small values of c, see Fig. 6(a.ii) for an illustration. The latter plateau determines the value of the susceptibility in the thermodynamic limit for $c \to 0$. In fact, this plateau extends to smaller values of c as N_σ increases and would end in a finite value if we take the limit $c \to 0$ after the thermodynamic limit.

To understand the second plateau in the susceptibility, which appears at small values of c in *finite* systems, it is instructive to recall how the effective potential can be reconstructed from the dependence of the external field on the magnetization, $c = c(\langle M \rangle_{V,c})$. Note that c increases strictly monotonically with $\langle M \rangle_{V,c}$ and we have $c \to 0$ for $\langle M \rangle_{V,c} \to 0$ in finite systems. Following our discussion of Eq. (49), the function $c(\langle M \rangle_{V,c})$ can be identified with the field derivative of the effective potential, $\partial_\varphi U$. Accordingly, the susceptibility $\sim \partial \langle M \rangle_{V,c} / \partial c$ can be related to the inverse of the curvature of the effective potential, $1/(\partial_\varphi^2 U)$. Starting

from large values of c, the rapid increase in the susceptibility to large values, accompanied by the formation of a plateau at small values of c, corresponds to a flattening of the effective potential for field values smaller than the one associated with the nontrivial minimum of the effective potential in the thermodynamic limit. Since convexity requires that the curvature of the effective potential must be zero for $|\varphi| < \langle M \rangle$ in the symmetry broken phase in the thermodynamic limit, the plateau of the susceptibility at small values of c must increase as N_σ increases. This is exactly what we observe in Fig. 6(a.ii).

For values of m^2 associated with a magnetization that vanishes in the thermodynamic limit for $c \to 0$, the curvature of the corresponding effective potential is finite and positive for all field values. As c is decreased, we therefore observe that the susceptibility only develops a single plateau in this case, see Fig. 6(b.ii). The height of this plateau determines the value of the susceptibility in the thermodynamic limit.

Three dimensions. Now we turn to the three-dimensional case which is most relevant from the standpoint of an analysis of finite-temperature phase transitions in $3+1$-dimensional spacetime.

In Fig. 7, the magnetization and the susceptibility are shown as functions of the external field c for various values of N_σ. As for the two-dimensional system, we show results for two values of the parameter m^2, one of which, $m^2 = -0.9$, is associated with the symmetry broken phase in the thermodynamic limit, while the other, $m^2 = -0.5$, is associated with the symmetric phase in the thermodynamic limit. Qualitatively, the magnetizations and susceptibilities associated with the two phases behave as their analogs in

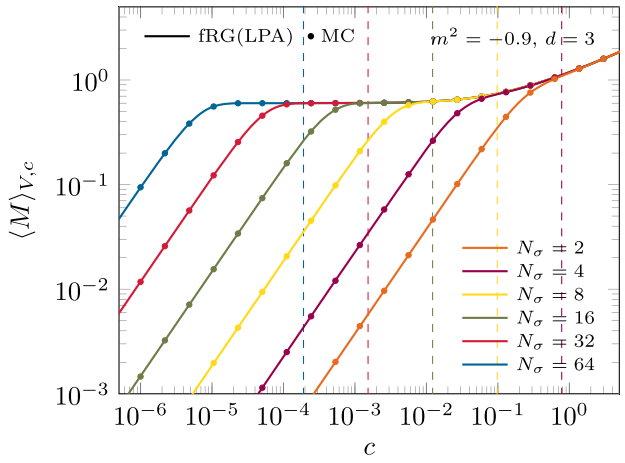

(a.i) Magnetization.

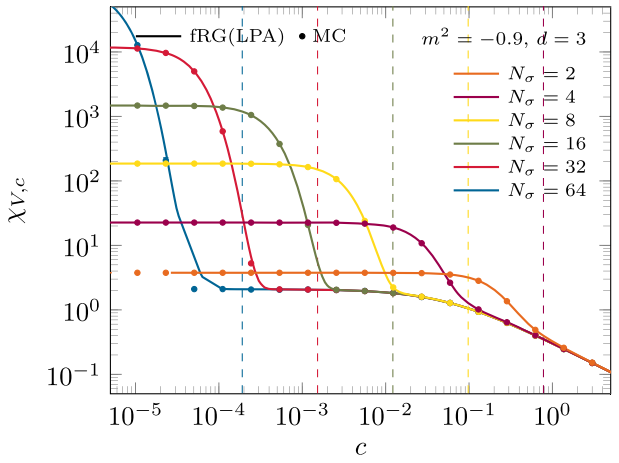

(a.ii) Susceptibility.

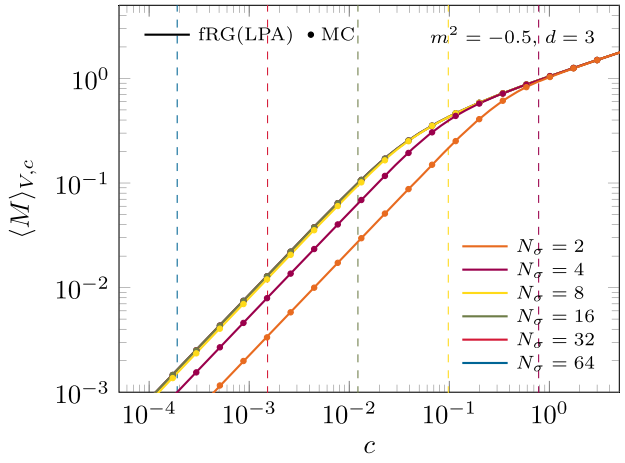

(b.i) Magnetization.

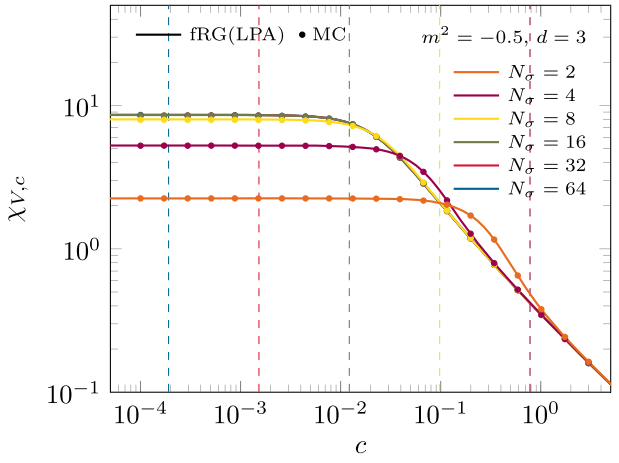

(b.ii) Susceptibility.

FIG. 7. Magnetization and susceptibility in three spacetime dimensions as a function of the external field c, as obtained from lattice MC (dots) and lattice fRG (solid lines) calculations, in panels (a.i) and (a.ii) for $m^2 = -0.9$, and in panels (b.i) and (b.ii) for $m^2 = -0.5$. The vertical dashed lines indicate the values of c at which the magnetization and susceptibility for the corresponding values of m^2 and N_σ have been extracted for our analysis of the m^2 dependence of these quantities in Fig. 9, see main text for details.

two dimensions. In fact, for $m^2 = -0.9$, we find the formation of a plateau in the magnetization as a function of the external field c. As we increase N_σ this plateau grows continuously and is expected to extend to $c = 0$ for $N_\sigma \to \infty$. This behavior signals that the magnetization remains finite in the thermodynamic limit, even in the absence of an external field. The susceptibility exhibits two plateaus as also observed for the two-dimensional system: one determining the susceptibility in the thermodynamic limit for $c \to 0$, and one indicating that the effective potential in the thermodynamic limit becomes flat for field values smaller than the one of the minimum. Again, we also observe that the limits $c \to 0$ and $N_\sigma \to \infty$ do not commute in the symmetry broken phase.

Let us now come to the case with $m^2 = -0.5$. Here, we do not observe the formation of a plateau in the magnetization as a function of the external field c as we increase N_σ. In fact, as we increase N_σ, we find that the magnetization converges to a continuous function which tends to zero for vanishing c. The susceptibility exhibits a similar convergent behavior and, as for the two-dimensional system, develops only a single plateau and approaches a finite value for $c \to 0$. This behavior of the magnetization and the susceptibility indicates that the $Z(2)$ symmetry is restored for $m^2 = -0.5$ in the thermodynamic limit.

Overall, we find that the lattice fRG and lattice MC results are in remarkable agreement, given the fact that the lattice fRG calculations are based on LPA. The reader may note apparent deviations of the lattice fRG results from the lattice MC results in the susceptibility for large values of N_σ and those values of c associated with the regime between the two plateaus. We emphasize that these deviations are only numerical artifacts of the lattice fRG calculations, which can in principle be removed by increasing the resolution of the grid in field space. For details on the numerical setup used for the lattice fRG calculations we refer the reader to Appendix A.

Finally, looking at our results for the magnetization and susceptibility in different numbers of spacetime dimensions, we find that the results obtained from lattice fRG in LPA and lattice MC are not only consistent on a qualitative level, but also become successively more consistent on a quantitative level as the number of dimensions increases. Without presenting numerical results here, we add that this is indeed confirmed by calculations of the magnetization and susceptibility in four spacetime dimensions.

3. Phase transitions

Above, we have discussed precursors of SSB in finite systems. In the following, we shall study the approach to phase transitions in two and three dimensions in the thermodynamic limit. This requires a calculation of the magnetization and the susceptibility as a function of the parameter m^2, which mimics the temperature in a thermodynamic system in one dimension higher.

However, before actually analyzing the transition from the symmetry broken to the symmetric phase, it is necessary to discuss briefly finite-volume effects which are present for small values of the external field c. Such effects become most pronounced for values of m^2 close to the phase transition (or crossover for finite c), as the correlation length becomes large in this regime. For example, this is the case for $m^2 = -1.5$ in two dimensions, see Figs. 6(a.i) and 6(a.ii), and for $m^2 = -0.9$ in three dimensions, see Figs. 7(a.i) and 7(a.ii).

To mimic properties of the system in the thermodynamic limit, we need to suppress finite-volume effects. This can be done by determining a specific value of the external field, $c_\star(N_\sigma)$, such that $\langle M\rangle_{V,c} \approx \langle M\rangle_c$ and $\chi_{V,c} \approx \chi_c$ for all $c \geq c_\star(N_\sigma)$ for a given d. Here, $\langle M\rangle_c$ and χ_c are the values of the magnetization and susceptibility in the thermodynamic limit in the presence of the external field c. Moreover, $c_\star(N_\sigma)$ should be chosen such that it is as small as possible and vanishes in the limit $N_\sigma \to \infty$. With this quantity at hand, we have

$$\langle M\rangle = \lim_{N_\sigma\to\infty} \langle M\rangle_{V,c_\star(N_\sigma)} \tag{50}$$

for a given d. Note that we shall determine $c_\star$ such that it does not depend on the bare parameters m^2 and λ.

To find an estimate for $c_\star$, we consider the susceptibility and determine the value of c at which finite-volume effects set in. For $d = 2$, we find that $c_\star(N_\sigma) = 10/(aN_\sigma)^2$ is an appropriate choice. For illustration, we show the corresponding values of $c_\star$ as vertical dashed lines in Figs. 6(a.i) and 6(a.ii). For $d = 3$, we obtain $c_\star(N_\sigma) = 50/(aN_\sigma)^3$, see the vertical dashed lines in Figs. 7(a.i) and 7(a.ii).

With $c_\star(N_\sigma)$ for two and three spacetime dimensions at hand, we can compute the magnetization and susceptibility as a function of the squared bare mass parameter m^2 to detect the formation of phase transitions in the thermodynamic limit. However, strictly speaking, phase transitions cannot occur in a finite system. The search for the emergence of nonanalyticities associated with phase transitions therefore requires an analysis of the scaling behavior of the magnetization and susceptibility with N_σ.

A detailed scaling analysis is beyond the scope of the present work. We shall only illustrate the scaling behavior of the magnetization and susceptibility in Figs. 8 and 9 for $d = 2$ and $d = 3$, respectively. In these figures, the magnetization $\langle M\rangle_{V,c}$ and the susceptibility $\chi_{V,c}$ are shown as functions of the squared (bare) mass m^2 for various values of N_σ. As explained above, the values of the external field c have been chosen such that $c = c_\star(N_\sigma) = 10/(aN_\sigma)^2$ for $d = 2$ and $c = c_\star(N_\sigma) = 50/(aN_\sigma)^3$ for $d = 3$. The vertical lines in Figs. 8 and 9 represent the values $m^2_{\text{peak}} \approx -1.295$ for $d = 2$ and $m^2_{\text{peak}} \approx -0.682$ for $d = 3$, respectively. These values correspond to the values of the bare mass where the fRG-intrinsic analysis of the predictive

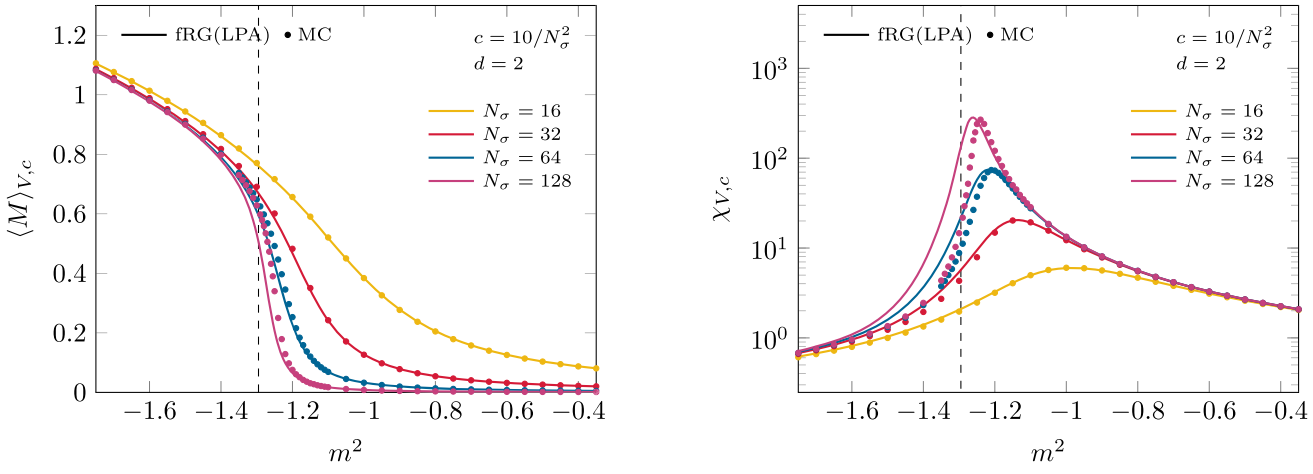

(a) Magnetization. (b) Susceptibility.

FIG. 8. Magnetization (a) and susceptibility (b) in two spacetime dimensions as a function of the bare mass for a fixed explicit symmetry breaking c, as obtained from lattice calculations (dots) and lattice-fRG calculations (solid lines). The vertical lines in the two panels indicate the position where our fRG-intrinsic analysis of the predictive power of LPA suggests the largest deviations from the exact solution, see Sec. VA.

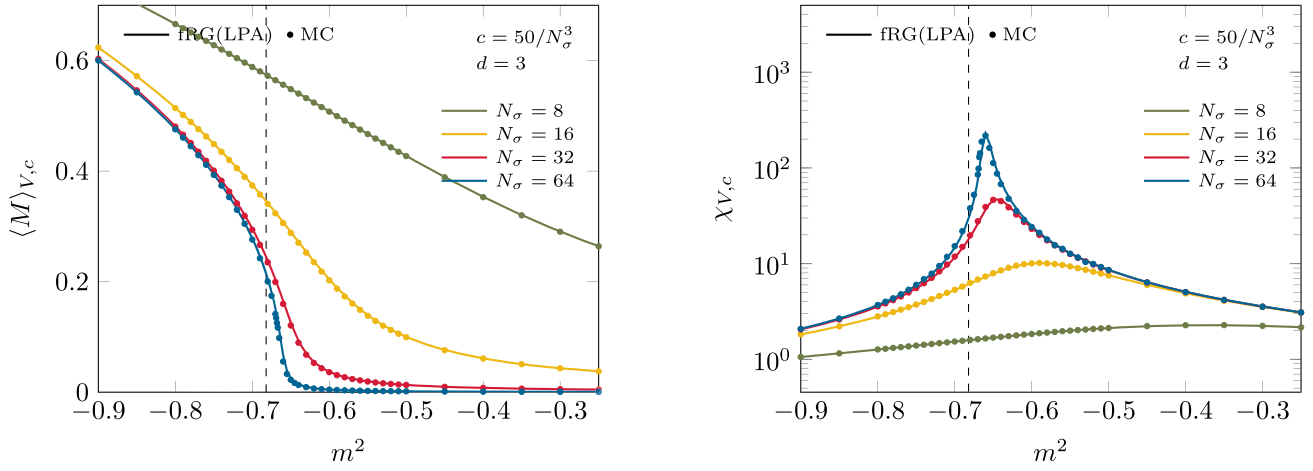

(a) Magnetization. (b) Susceptibility.

FIG. 9. Magnetization (a) and susceptibility (b) in three spacetime dimensions as a function of the bare mass for a fixed explicit symmetry breaking c, as obtained from lattice calculations (dots) and lattice-fRG calculations (solid lines). The vertical lines in the two panels indicate the position where our fRG-intrinsic analysis of the predictive power of LPA suggests the largest deviations from the exact solution, see Sec. VA.

power of LPA suggests the largest deviations from the exact solution, see Sec. VA. Note that these values should not be confused with the critical bare mass value associated with the phase transition in the thermodynamic limit.

For $d = 2$ and $d = 3$, we observe a behavior of the magnetization and susceptibility in Figs. 8 and 9, which is indicative of a second-order phase transition: the magnetization develops a pronounced kink as N_σ increases, and the susceptibility increases with N_σ, indicating the formation of a divergence.

Comparing the results for the magnetization and susceptibility from our lattice fRG studies in LPA with those from our lattice MC calculations, we find excellent agreement for small N_σ. In the symmetric phase, this appears to hold even for larger values of N_σ. However, for $d = 2$, significant deviations appear in the symmetry broken phase, see Appendix B for a more detailed analysis. This observation is in accordance with our fRG-intrinsic analysis of the predictive power of LPA in Sec. VA. In fact, this analysis already indicates that the deviations of the lattice fRG results in LPA from the exact solution should be expected to be larger in $d = 2$ than in $d = 3$. Note that the deviations in the magnetization and susceptibility are indeed maximal around $m^2 = m^2_{\text{peak}}$, as predicted by our

fRG-intrinsic analysis. Apparently, m^2_{peak} is close to the phase transition in both $d = 2$ and $d = 3$.

We conclude this section by adding that the good agreement between the results of our lattice fRG calculations in LPA and lattice MC studies in $d = 3$ is also not unexpected from a more general standpoint. In fact, the anomalous dimension η, which can be viewed as a measure of the relevance of nontrivial momentum dependences in correlation functions, is small at the phase transition in $d = 3$, $\eta \approx 0.036$, see, e.g., Refs. [61,64,65]. In LPA, we have $\eta = 0$ by construction, regardless of the dimension of the system. It is then also reasonable that the situation is different in two spacetime dimensions. There, the anomalous dimension is about an order of magnitude larger than in three spacetime dimensions [61], indicating the relevance of nontrivial momentum structures in, e.g., the propagator. From a more phenomenological standpoint, the potential relevance of nontrivial momentum dependences close to the phase transition appears reasonable since the particles associated with our quantum field become massless at the phase transition. Away from the transition, both in the symmetry broken and symmetric phase, the masses of these particles are finite which suppresses momentum dependences in correlation functions. This is indeed confirmed by the particularly good agreement between our results of lattice MC and lattice fRG in LPA away from the phase transition.

VI. CONCLUSION

In the present work, we have introduced a framework for a direct comparison of lattice MC and lattice fRG studies on finite volumes and at fixed lattice spacing, thus avoiding any nontrivial parameter matching between the two. In particular, this allows for a clear analysis of a wide range of artifacts, such as cutoff, finite-volume, and truncation effects.

As a first application of our framework, we have considered a scalar $Z(2)$ theory in various spacetime dimensions and provided detailed comparisons for the magnetization, the susceptibility, and phase transitions. For a given size of the spacetime lattice, and at fixed lattice spacing, the lattice MC results contain only statistical errors, which for these simple systems can be made arbitrarily small. In such a situation, our framework is ideally suited to analyze the predictive power of truncations entering the computations within the fRG approach. In the present work, we have demonstrated this by comparing lattice MC results with results from lattice fRG calculations in LPA. Within the fRG approach, this is the simplest approximation that already takes into account fluctuation effects. Indeed, this approximation of the effective action at leading order in a derivative expansion has been widely used in the past and is still frequently used in various research fields.

For a small number of lattice sites, we have found that the lattice fRG results in LPA are in excellent agreement with our MC results, regardless of the number of spacetime dimensions. We have shown that this follows from the fact that LPA becomes exact in the limit of a lattice consisting of only a single spacetime point. By increasing the number of lattice sites, we have observed that the results for the magnetization and susceptibility from the two methods start to deviate in regimes associated with a small mass of the field, e.g., close to the phase transition in two and three spacetime dimensions, but still remain in agreement at a qualitative level. The size of the aforementioned deviations depends on the number of spacetime dimensions. In general, however, our results indicate that the deviations become smaller as the number of spacetime dimensions increases, such that the lattice fRG results in LPA and the lattice MC results become successively more consistent on a quantitative level. In fact, while the deviations in the magnetization and especially in the susceptibility are still significant around the phase transition in two spacetime dimensions, the lattice fRG and lattice MC results show remarkable agreement in three spacetime dimensions, away from the phase transition but also close to it. Given the simplicity of LPA, this is indeed impressive. Our analysis indicates that this can be traced back to the fact that nontrivial momentum dependences in the correlation functions become less relevant in higher dimensions, at least with respect to calculations of the magnetization and susceptibility. This observation is consistent with the anomalous dimension at the phase transition being one order of magnitude smaller in three spacetime dimensions than in two spacetime dimensions.

In addition to testing the predictive power of fRG approximation schemes, as exemplified in our present work, it may be beneficial for lattice MC studies to exploit the fact that lattice fRG calculations can be used to track the scaling behavior of observables from very small lattices up to the thermodynamic limit, as well as the approach to the continuum limit. For example, provided that the results of both methods are found to agree well over a range of lattice sizes, our lattice fRG approach can be used to guide extrapolations of lattice MC data. This may be relevant for theories with fermions or for tests of methods developed to surmount the sign problem at finite density. Conversely, the very good agreement of our lattice fRG results in LPA and lattice MC results over a wide range of lattice sizes indicates that large lattices may be required to resolve the effect of nontrivial momentum dependences of correlation functions on observables, e.g., in the critical regime.

In general, the opportunity to make clear and meaningful comparisons of lattice MC and fRG studies offers great potential, as it may lead to cross-fertilization and improvements on both sides in the future.

ACKNOWLEDGMENTS

We thank A. Koenigstein, J. M. Pawlowski, and J. Stoll for discussions and comments on the manuscript.

This work is supported by the Deutsche Forschungsgemeinschaft (DFG, German Research Foundation) through the CRC-TR 211 "Strong-interaction matter under extreme conditions"—Project Number 315477589–TRR 211 and by the State of Hesse within the Research Cluster ELEMENTS (Project No. 500/10.006).

DATA AVAILABILITY

The data that support the findings of this article are openly available [68].

APPENDIX A: NUMERICAL IMPLEMENTATION OF THE FRG FLOW EQUATION OF THE EFFECTIVE POTENTIAL

To solve the flow equation for the effective potential, which is a highly nonlinear diffusion equation, we have brought it into a conservative form by taking a field derivative of it [56,69]. The resulting equation can then be solved by using a so-called finite-volume method based on the Kurganov-Tadmor scheme, see Ref. [70]. In the present work, we have used the same semidiscrete implementation as described in Refs. [56,59]. For the numerical time stepper, we have used SOLVE_IVP with LSODA and $a_{\mathrm{tol}} = r_{\mathrm{tol}} = 10^{-14}$ for its absolute and relative tolerances, respectively, if not stated otherwise. To obtain the numerical results shown in Figs. 1–4, we have moreover used an equidistant grid in field space with spacing $\Delta\varphi = 0.001$, while we have used $\Delta\varphi = 0.0001$ to obtain the results shown in all other figures. For the maximal field value, we have used $\varphi_{\mathrm{max}} = 3$ for $d = 2, 3$ and $\varphi_{\mathrm{max}} = 5$ for $d = 1$. At the boundaries in field space, we have followed Ref. [56] and employed a linear extrapolation at $\varphi = 0$ and $\varphi = \varphi_{\mathrm{max}}$. For the initial RG scale Λ, we have used $\Lambda = 100/a$ in all numerical calculations, which effectively removes the dependence of our results from this scale. This is in accordance with our discussion in Sec. IV where we show that the limit $\Lambda \to \infty$ can be taken for a given finite lattice spacing a. In the IR regime, we have always stopped the RG flow at $k/\Lambda = k_{\mathrm{IR}}/\Lambda = 10^{-12}$.

APPENDIX B: EXTERNAL FIELD DEPENDENCE CLOSE TO THE PHASE TRANSITION IN TWO SPACETIME DIMENSIONS

In Sec. V B 2, we have discussed the dependence of the magnetization and susceptibility on the external field c for two values of the squared (bare) mass parameter m^2 in two spacetime dimensions, see Fig. 6. The results in this figure show that the lattice MC results and the lattice fRG results in LPA agree well for both values of m^2. Deviations in the susceptibility emerge only for very large lattices close to the phase transition. However, this observation is somewhat misleading as suggested by Fig. 8. There, our results for the magnetization and susceptibility are shown as a function of m^2. From this figure, we deduce that the results obtained with the two methods do not agree in the vicinity of the phase transition.

In Fig. 10, we show the magnetization and susceptibility as a function of the external field c again, but now for $m^2 = m^2_{\mathrm{peak}} \approx -1.295$ (vertical dashed line in Fig. 8). At this value of m^2, we have the greatest deviation of the lattice fRG and lattice MC results in Fig. 8, in accordance with our fRG-intrinsic analysis of the predictive power of LPA in Sec. V A. We observe in Fig. 10 that the lattice fRG and

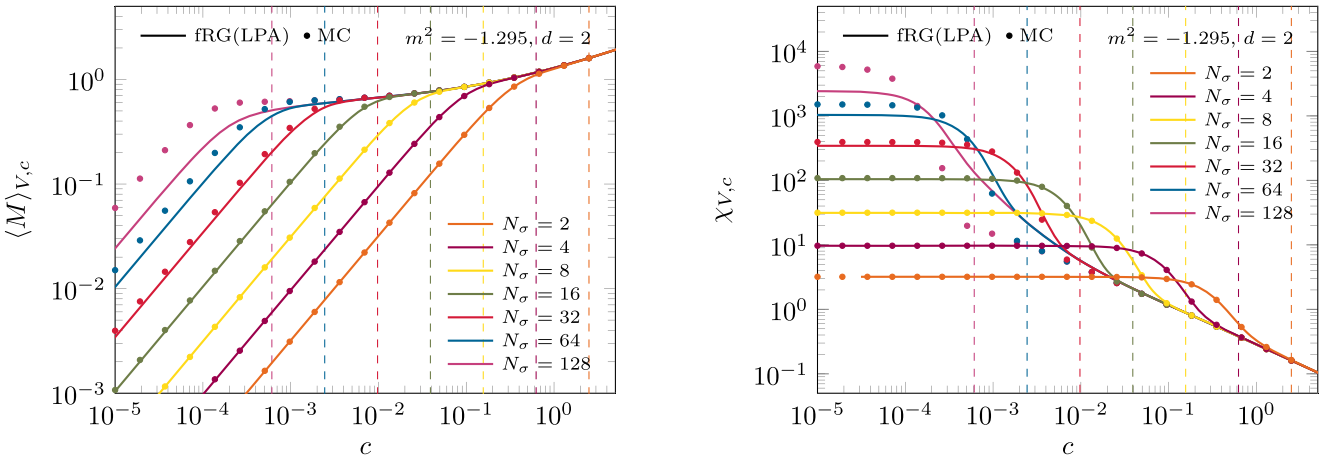

(a) Magnetization. (b) Susceptibility.

FIG. 10. Magnetization (a) and susceptibility (b) in two spacetime dimensions from lattice MC (dots) and lattice fRG (solid lines) calculations as a function of the external field c at $m^2 = m^2_{\mathrm{peak}} \approx -1.295$. At this value of m^2, the greatest discrepancy of the lattice fRG results in LPA and lattice MC results is observed, see vertical dashed line in Fig. 8. The vertical dashed lines again indicate the values of c at which the magnetization and susceptibility for the corresponding values of m^2 and N_σ have been extracted for our analysis of the m^2 dependence of these quantities in Fig. 8.

lattice MC results for $m^2 = m^2_{\text{peak}}$ deviate from each other over a wide range of external field values, down to smaller and smaller values of c as N_σ increases. In particular, we find that the deviations already appear on comparatively small lattices. For sufficiently large values of c, the results from the two methods are in good agreement. However, this is not surprising: fluctuation effects and momentum dependences in correlation functions are suppressed in this regime since the mass of the scalar field increases with c.

Recall that the magnetization as a function of the external field is directly related to the field derivative of the effective potential as a function of the field, see Sec. V B 1. Thus, the deviations of the lattice fRG results for the magnetization at small c from the lattice MC results would translate into corresponding deviations in the predictions for the effective potential near its minimum and at small field values.

We emphasize that the deviations in the results from the two methods are (strongly) suppressed (far) away from the critical region in two spacetime dimensions, see, e.g., Fig. 8. In any case, the deviations are generally much smaller in three spacetime dimensions, even near the phase transition, see, e.g., Fig. 9.

[1] A. Bazavov *et al.* (HotQCD Collaboration), Chiral crossover in QCD at zero and non-zero chemical potentials, Phys. Lett. B **795**, 15 (2019).

[2] C. Bonati, M. D'Elia, F. Negro, F. Sanfilippo, and K. Zambello, Curvature of the pseudocritical line in QCD: Taylor expansion matches analytic continuation, Phys. Rev. D **98**, 054510 (2018).

[3] H. T. Ding *et al.* (HotQCD Collaboration), Chiral phase transition temperature in $(2+1)$-flavor QCD, Phys. Rev. Lett. **123**, 062002 (2019).

[4] C. Bonati, E. Calore, M. D'Elia, M. Mesiti, F. Negro, F. Sanfilippo, S. F. Schifano, G. Silvi, and R. Tripiccione, Roberge-Weiss endpoint and chiral symmetry restoration in $N_f = 2+1$ QCD, Phys. Rev. D **99**, 014502 (2019).

[5] S. Borsanyi, Z. Fodor, J. N. Guenther, R. Kara, S. D. Katz, P. Parotto, A. Pasztor, C. Ratti, and K. K. Szabo, QCD crossover at finite chemical potential from lattice simulations, Phys. Rev. Lett. **125**, 052001 (2020).

[6] Y. Kuramashi, Y. Nakamura, H. Ohno, and S. Takeda, Nature of the phase transition for finite temperature $N_{\text{f}} = 3$ QCD with nonperturbatively $\text{O}(a)$ improved wilson fermions at $N_{\text{t}} = 12$, Phys. Rev. D **101**, 054509 (2020).

[7] A. Y. Kotov, M. P. Lombardo, and A. Trunin, QCD transition at the physical point, and its scaling window from twisted mass Wilson fermions, Phys. Lett. B **823**, 136749 (2021).

[8] A. Y. Kotov, M. P. Lombardo, and A. Trunin, Gliding down the QCD transition line, from $N_f = 2$ till the onset of conformality, Symmetry **13**, 1833 (2021).

[9] F. Cuteri, O. Philipsen, and A. Sciarra, On the order of the QCD chiral phase transition for different numbers of quark flavours, J. High Energy Phys. 11 (2021) 141.

[10] L. Dini, P. Hegde, F. Karsch, A. Lahiri, C. Schmidt, and S. Sharma, Chiral phase transition in three-flavor QCD from lattice QCD, Phys. Rev. D **105**, 034510 (2022).

[11] F. Cuteri, J. Goswami, F. Karsch, A. Lahiri, M. Neumann, O. Philipsen, C. Schmidt, and A. Sciarra, Toward the chiral phase transition in the Roberge-Weiss plane, Phys. Rev. D **106**, 014510 (2022).

[12] A. D'Ambrosio, O. Philipsen, and R. Kaiser, The chiral phase transition at non-zero imaginary baryon chemical potential for different numbers of quark flavours, *Proc. Sci.*, LATTICE2022 (2023) 172 [arXiv:2212.03655].

[13] H.-T. Ding, W.-P. Huang, S. Mukherjee, and P. Petreczky, Microscopic encoding of macroscopic universality: Scaling properties of Dirac eigenspectra near QCD chiral phase transition, Phys. Rev. Lett. **131**, 161903 (2023).

[14] H. T. Ding, O. Kaczmarek, F. Karsch, P. Petreczky, M. Sarkar, C. Schmidt, and S. Sharma, Curvature of the chiral phase transition line from the magnetic equation of state of $(2+1)$-flavor QCD, Phys. Rev. D **109**, 114516 (2024).

[15] J. P. Klinger, R. Kaiser, and O. Philipsen, The order of the chiral phase transition in massless many-flavour lattice QCD, *Proc. Sci.*, LATTICE2024 (2025) 172 [arXiv:2501.19251]

[16] Y. Zhang, Y. Aoki, S. Hashimoto, I. Kanamori, T. Kaneko, and Y. Nakamura, Three flavor QCD phase transition with Möbius domain wall fermions, *Proc. Sci.*, LATTICE2024 (2025) 193 [arXiv:2501.15494].

[17] S. Borsanyi, Z. Fodor, J. N. Guenther, P. Parotto, A. Pasztor, C. Ratti, V. Vovchenko, and C. H. Wong, Lattice QCD constraints on the critical point from an improved precision equation of state, arXiv:2502.10267.

[18] W.-j. Fu, J. M. Pawlowski, and F. Rennecke, QCD phase structure at finite temperature and density, Phys. Rev. D **101**, 054032 (2020).

[19] J. Braun, W.-j. Fu, J. M. Pawlowski, F. Rennecke, D. Rosenblüh, and S. Yin, Chiral susceptibility in $(2+1)$-flavor QCD, Phys. Rev. D **102**, 056010 (2020).

[20] F. Gao and J. M. Pawlowski, Chiral phase structure and critical end point in QCD, Phys. Lett. B **820**, 136584 (2021).

[21] F. Gao and J. M. Pawlowski, Phase structure of $(2+1)$-flavor QCD and the magnetic equation of state, Phys. Rev. D **105**, 094020 (2022).

[22] P. J. Gunkel and C. S. Fischer, Locating the critical endpoint of QCD: Mesonic backcoupling effects, Phys. Rev. D **104**, 054022 (2021).

[23] J. Braun *et al.*, Soft modes in hot QCD matter, Phys. Rev. D **111**, 094010 (2025).

[24] W.-j. Fu, X. Luo, J. M. Pawlowski, F. Rennecke, and S. Yin, Ripples of the QCD critical point, Phys. Rev. D **111**, L031502 (2025).

[25] J. Bernhardt and C. S. Fischer, QCD phase transitions in the light quark chiral limit, Phys. Rev. D **108**, 114018 (2023).
[26] C. S. Fischer, QCD at finite temperature and chemical potential from Dyson–Schwinger equations, Prog. Part. Nucl. Phys. **105**, 1 (2019).
[27] N. Dupuis, L. Canet, A. Eichhorn, W. Metzner, J. M. Pawlowski, M. Tissier, and N. Wschebor, The nonperturbative functional renormalization group and its applications, Phys. Rep. **910**, 1 (2021).
[28] O. Philipsen, Lattice constraints on the QCD chiral phase transition at finite temperature and baryon density, Symmetry **13**, 2079 (2021).
[29] G. Aarts *et al.*, Phase transitions in particle physics: Results and perspectives from lattice quantum chromo-dynamics, Prog. Part. Nucl. Phys. **133**, 104070 (2023).
[30] J. Braun, B. Klein, and H. J. Pirner, Volume dependence of the pion mass in the quark-meson-model, Phys. Rev. D **71**, 014032 (2005).
[31] J. Braun, B. Klein, and H. J. Pirner, Influence of quark boundary conditions on the pion mass in finite volume, Phys. Rev. D **72**, 034017 (2005).
[32] J. Braun and B. Klein, Finite-size scaling behavior in the O(4)-model, Eur. Phys. J. C **63**, 443 (2009).
[33] L. Fister and J. M. Pawlowski, Functional renormalization group in a finite volume, Phys. Rev. D **92**, 076009 (2015).
[34] L. Batini, E. Grossi, and N. Wink, Dissipation dynamics of a scalar field, Phys. Rev. D **108**, 125021 (2023).
[35] N. Dupuis and K. Sengupta, Non-perturbative renormalization-group approach to lattice models, Eur. Phys. J. B **66**, 271 (2008).
[36] T. Machado and N. Dupuis, From local to critical fluctuations in lattice models: A non-perturbative renormalization-group approach, Phys. Rev. E **82**, 041128 (2010).
[37] A. Rancon and N. Dupuis, Nonperturbative renormalization-group approach to strongly-correlated lattice bosons, Phys. Rev. B **84**, 174513 (2011).
[38] J. Krieg and P. Kopietz, Dual lattice functional renormalization group for the Berezinskii-Kosterlitz-Thouless transition: irrelevance of amplitude and out-of-plane fluctuations, Phys. Rev. E **96**, 042107 (2017).
[39] J. M. Pawlowski, I.-O. Stamatescu, and F. P. G. Ziegler, Cooling stochastic quantization with colored noise, Phys. Rev. D **96**, 114505 (2017).
[40] S. Duane, A. Kennedy, B. J. Pendleton, and D. Roweth, Hybrid Monte Carlo, Phys. Lett. B **195**, 216 (1987).
[41] J. Braun, B. Klein, and P. Piasecki, On the scaling behavior of the chiral phase transition in QCD in finite and infinite volume, Eur. Phys. J. C **71**, 1576 (2011).
[42] J. Braun, B. Klein, and B.-J. Schaefer, On the phase structure of QCD in a finite volume, Phys. Lett. B **713**, 216 (2012).
[43] R.-A. Tripolt, J. Braun, B. Klein, and B.-J. Schaefer, Effect of fluctuations on the QCD critical point in a finite volume, Phys. Rev. D **90**, 054012 (2014).
[44] B. Klein, Modeling finite-volume effects and chiral symmetry breaking in two-flavor QCD thermodynamics, Phys. Rep. **707–708**, 1 (2017).
[45] C. Wetterich, Exact evolution equation for the effective potential, Phys. Lett. B **301**, 90 (1993).
[46] J. M. Pawlowski, Aspects of the functional renormalisation group, Ann. Phys. (Amsterdam) **322**, 2831 (2007).
[47] J. Berges, N. Tetradis, and C. Wetterich, Nonperturbative renormalization flow in quantum field theory and statistical physics, Phys. Rep. **363**, 223 (2002).
[48] H. Gies, Introduction to the functional RG and applications to gauge theories, Lect. Notes Phys. **852**, 287 (2012).
[49] B. Delamotte, An Introduction to the nonperturbative renormalization group, Lect. Notes Phys. **852**, 49 (2012).
[50] P. Kopietz, L. Bartosch, and F. Schütz, Introduction to the functional renormalization group, Lect. Notes Phys. **798**, 1 (2010).
[51] J. Braun, Fermion interactions and universal behavior in strongly interacting theories, J. Phys. G **39**, 033001 (2012).
[52] J. Braun, M. Leonhardt, and J. M. Pawlowski, Renormalization group consistency and low-energy effective theories, SciPost Phys. **6**, 056 (2019).
[53] D. F. Litim, Optimized renormalization group flows, Phys. Rev. D **64**, 105007 (2001).
[54] D. F. Litim, Mind the gap, Int. J. Mod. Phys. A **16**, 2081 (2001).
[55] J. Keitel and L. Bartosch, The zero-dimensional O(N) vector model as a benchmark for perturbation theory, the large-N expansion and the functional renormalization group, J. Phys. A **45**, 105401 (2012).
[56] A. Koenigstein, M. J. Steil, N. Wink, E. Grossi, J. Braun, M. Buballa, and D. H. Rischke, Numerical fluid dynamics for FRG flow equations: Zero-dimensional QFTs as numerical test cases. I. The O(N) model, Phys. Rev. D **106**, 065012 (2022).
[57] A. Koenigstein, M. J. Steil, N. Wink, E. Grossi, and J. Braun, Numerical fluid dynamics for FRG flow equations: Zero-dimensional QFTs as numerical test cases. II. Entropy production and irreversibility of RG flows, Phys. Rev. D **106**, 065013 (2022).
[58] M. J. Steil and A. Koenigstein, Numerical fluid dynamics for FRG flow equations: Zero-dimensional QFTs as numerical test cases. III. Shock and rarefaction waves in RG flows reveal limitations of the $N \to \infty$ limit in O(N)-type models, Phys. Rev. D **106**, 065014 (2022).
[59] N. Zorbach, A. Koenigstein, and J. Braun, Functional renormalization group meets computational fluid dynamics: RG flows in a multi-dimensional field space, arXiv:2412.16053.
[60] N. Zorbach, J. Stoll, and J. Braun, Optimization and stabilization of functional renormalization group flows, Phys. Rev. D **111**, 096022 (2025).
[61] A. Pelissetto and E. Vicari, Critical phenomena and renormalization group theory, Phys. Rep. **368**, 549 (2002).
[62] D. F. Litim and D. Zappala, Ising exponents from the functional renormalisation group, Phys. Rev. D **83**, 085009 (2011).
[63] D. F. Litim, Critical exponents from optimized renormalization group flows, Nucl. Phys. **B631**, 128 (2002).
[64] F. Benitez, J. P. Blaizot, H. Chate, B. Delamotte, R. Mendez-Galain, and N. Wschebor, Solutions of renormalization group flow equations with full momentum dependence, Phys. Rev. E **80**, 030103 (2009).
[65] F. Benitez, J. P. Blaizot, H. Chate, B. Delamotte, R. Mendez-Galain, and N. Wschebor, Non-perturbative renormalization group preserving full-momentum dependence: Implementation

and quantitative evaluation, Phys. Rev. E **85**, 026707 (2012).

[66] F. Murgana, A. Koenigstein, and D. H. Rischke, Reanalysis of critical exponents for the O(N) model via a hydrodynamic approach to the functional renormalization group, Phys. Rev. D **108**, 116016 (2023).

[67] A. S. Kapoyannis and N. Tetradis, Quantum mechanical tunneling and the renormalization group, Phys. Lett. A **276**, 225 (2000).

[68] N. Zorbach, J.-P. Klinger, Owe Philipsen, and J. Braun, Lattice Monte Carlo meets lattice functional Renormalization group: A quantitative comparison, arXiv:2503.14149.

[69] E. Grossi and N. Wink, Resolving phase transitions with Discontinuous Galerkin methods, SciPost Phys. Core **6**, 071 (2023).

[70] A. Kurganov and E. Tadmor, New high-resolution central schemes for nonlinear conservation laws and convection–diffusion equations, J. Comput. Phys. **160**, 241 (2000).